A NEW TECHNIQUE FOR NANOLITHOGRAPHY USING ELECTROHYDRODYNAMIC METHOD AND ARGON ION ETCHING PROCESS

HİLAL DÖĞER

Master's Thesis

Graduate School
Izmir University of Economics
İzmir
2021

A NEW TECHNIQUE FOR NANOLITHOGRAPHY USING ELECTROHYDRODYNAMIC METHOD AND ARGON ION ETCHING PROCESS

HİLAL DÖĞER

A Thesis Submitted to
The Graduate School of Izmir University of Economics
Master's Program in Bioengineering

Izmir
2021

ABSTRACT

A NEW TECHNIQUE FOR NANOLITHOGRAPHY USING ELECTROHYDRODYNAMIC METHOD AND ARGON ION ETCHING PROCESS

Döğer, Hilal

Master's Program in Bioengineering

Advisor: Asst. Prof. Dr. Özge Sağlam

August, 2021

Various lithography techniques are used in the production of devices that require micro and nano structure. Nowadays, multi-stage processes or high-cost problems can be encountered in the lithography methods used. Nanofibers, which can be obtained from various polymers and have high elasticity, are frequently used in device development. In the electrohydrodynamic method nanofibers can be produced in desired composition and diameter and can be easily controlled at close range has caused them to be frequently preferred. The objective of this thesis is developing a new type of nanolithography technique using the electrohydrodynamic method and argon ion etching process. First, nanofibers were patterned on silicon and glass substrates thermally coated with chromium, silver and gold. Afterwards, metallic patterns were developed by applying argon ion etching and polymer removal processes to the patterned structures, respectively. The electrical characterization of the metallic

patterns was carried out by the two-probe method. The morphology of the patterns was obtained by Atomic Force Microscopy before and after the removal of polymer process. The elemental analysis of the structures was performed by Scanning Electron Microscopy-EDX. The various metallic patterns including interdigitated structures were successfully produced with nanofibers on the substrates by optimizing the system parameters. Consequently, while nanofibers were produced for use in previous studies, a new nanolithography method was developed by using nanofibers as a *tool* in this thesis.

Keywords: Near-field electrospinning, nanofiber, nanolithography, direct writing, electrohydrodynamic method

ÖZET

ELEKTROHİDRODİNAMİK YÖNTEM VE ARGON İYON AŞINDIRMA İŞLEMLERİ KULLANILARAK NANOLİTOGRAFİ İÇİN YENİ BİR TEKNİK GELİŞTİRİLMESİ

Döğer, Hilal

Biyomühendislik Yüksek Lisans Programı

Tez Danışmanı: Dr. Öğr. Üyesi Özge Sağlam

Ağustos, 2021

Mikro ve nano yapı gerektiren cihazlar için çeşitli litografi teknikleri kullanılmaktadır. Günümüzde kullanılan litografi yöntemlerinde çok aşamalı prosesler veya yüksek maliyet sorunlarıyla karşılaşılabilmektedir. Çeşitli polimerlerden elde edilebilen ve yüksek elastikiyete sahip olan nanofiberler, cihaz geliştirmede sıklıkla kullanılmaktadır. Elektroeğirme yöntemi, nanofiberlerin istenilen kompozisyon ve çapta üretilebilmesi ve yakın mesafede kontrol edilerek desenlenebilmeleri nedeniyle, araştırmacılar tarafından sıklıkla tercih edilmektedir. Bu tezin amacı, elektrohidrodinamik yöntem ile üretilen nanofiberler ve argon iyon aşındırma işlemini kullanarak yeni bir tür nanolitografi tekniği geliştirmektir. İlk aşamada nanofiberler, termal buharlaştırma ile krom, gümüş ve altın ile kaplanmış silikon ve cam alttaşlar üzerine desenlendi. Sonrasında desenlenmiş yapılara sırasıyla argon iyon aşındırma ve polimer kaldırma işlemleri uygulanarak metalik desenler üretildi. Metalik desenlerin

elektriksel karakterizasyonu, iki nokta ölçüm yöntemiyle gerçekleştirildi. Desenlerin morfolojisi, kaldırma işleminden önce ve sonra Atomik Kuvvet Mikroskobu ile elde edildi. Yapıların element analizi, Taramalı Elektron Mikroskobu-EDX ile yapıldı. Sistem parametrelerinin optimize edilmesiyle, nanofiberler ile alttaşlar üzerinde birbirine bağlı interdigitated yapıları içeren çeşitli metalik desenler başarılı bir şekilde üretildi. Sonuç olarak, nanofiberler önceki çalışmalarda kullanılmak için üretilirken, bu tezde nanofiberler bir araç olarak kullanılarak yeni bir nanolitografi yöntemi geliştirildi.

Anahtar Kelimeler: Yakın mesafeli elektro-eğirme, nanofiber, nanolitografi, direkt yazma, elektrohidrodinamik yöntem

To my precious family who always support me…

ACKNOWLEDGEMENTS

First of all, I would like to thank my valuable advisor, Asst. Prof. Dr. Özge Sağlam, for giving me the opportunity to do research and providing invaluable guidance throughout this research. Her determination, knowledge, enthusiasm and desire for science, dynamism, vision, sincerity and motivation have deeply inspired me. She has taught me the methodology to carry out the research and to present the research works. It was a great privilege and honor to work and study under her guidance. I am extremely grateful for what she has offered me.

In addition, I would like to express my sincere thanks to Prof. Dr. Lütfi Özyüzer who helped me in my studies, provided work opportunities for the thesis, and guided me with his experiences. I would like to thank Prof. Dr. Gülnur Aygün, Mehtap Özdemir Köklü, Yasemin Demirhan for their contributions and development of my thesis. My special thanks go to Aileen Noori for helping the experiments.

My sincere thanks to the Scientific and Technological Council of Turkey (TUBITAK) for award-winning support 2211-National Graduate Scholarship Program (2210-C National MSc Program in the Priority Fields in Science and Technology) and financial supports (Grant number; 217M144). Besides that, I would like to thank the Research and Application Center for Quantum Technologies (RACQUT).

I am extremely grateful to my parents for their love, prayers, caring and sacrifices for educating and preparing me for my future. I am very much thankful to my sister, Ayşenur Döğer, and my dear Caner Erdoğdu for their love, understanding, prayers, and continuing support to complete this research work. Also, I express my thanks to my dear sister Ece Bozkır and my dear brothers, Ahmet Fatih Döğer and Fetih Can Döğer for their support and valuable prayers.

A special thanks goes to my lab mate Bensu Günay for endless support. In addition, I would like to thank to Hüseyin Saygın Portakal, Özge Süer, İrem Ceren Özen, Begümnur Küçükcan, Ceren Nisa Uysal, Ilgaz Çavuşoğlu, Hazal Gül, Sıla Köse, Burçin Dersu Açıkgöz for their motivation, help and endless support.

I would also like to express my special thanks to my dear friends Betül Kırmızıgül, Alexandra Rengin Bıçakçı, Füsun Sarıgül, Özlem Mahmutoğulları, who supported me in my difficult times and gave me happiness and hope.

TABLE OF CONTENTS

LIST OF TABLES

LIST OF FIGURES

LIST OF ABBREVIATIONS

AFM: Atomic Force Microscopy

Ar: Argon

AZO: Aluminum-doped zinc oxide

EB: Electron beam lithography

EDX: Energy Dispersive X-ray

EHD: Electrohydrodynamic

HSQ: Hydrogen silsesquioxane

IBE: Ion Beam Etching

MB: Melt Blown

MEMS: Microelectromechanical systems

NEMS: Nanoelectromechanical systems

PEO: Polyethylene oxide

PLLA: Poly (L-lactic acid)

PMMA: Polymethyl methacrylate

PVD: Physical Deposition System

PVP: Polyvinylpyrrolidone

RACQUT: Research and Application Center for Quantum Technologies

SEM: Scanning Electron Microscopy

SiO_2 : Silicon dioxide

SPL: Scanning Probe Lithography

SPU: steps per unit

STM: Scanning Tunneling Microscopy

UV: Ultraviolet

VOx: Vanadium oxide

CHAPTER 1: INTRODUCTION

1.1. Nanofabrication Techniques

In this thesis, an alternative method to nanolithography techniques was developed. In this regard, commonly used nanolithography techniques are described in this section.

Nanomaterials affiliate electrical, optical, magnetic, and mechanical properties to the material (Wu et al., 2020). The development of new generation technologies by using these features has been the focus of academic and industrial areas. In the last fifty years, studies have been made about the synthesis of nanostructures in various content and geometries with the bottom-up approaches and the formation of nanostructures from three-dimensional bulk structures with various top-down approaches.

Focusing on the production of micro and nano-sized structures is an important factor in the development of modern sciences and technologies. Microelectromechanical systems (MEMs), sensors, and microanalytical systems are produced with micro/nanotechnology applications. These practices are expected to significantly improve our workforce (Pimpin and Srituravanich, 2012). Recently, these production techniques have been emphasized and successful results have been achieved (Li et al., 2013).

1.1.1. Nanolithography

Conventional lithography is one of the techniques in which this approach is adopted. Nanolithography techniques, which are at the forefront of conventional nanopatterning techniques, are also used in the semiconductor industry (Kim et al., 2013).

Nanolithography fabricates structures in which at least one horizontal dimension is in nanometer scale. It is a branch of nanotechnology that deals with the study and applications of nanomanufacturing of nanometer-scale structures. Nanolithography is used for applications involving various scientific disciplines in nanoelectromechanical systems (NEMS), nano-fabrication of semiconductor

integrated circuits, (Ruiz and Chen, 2007), or any other nano research like fabrication of nanoscale stacked-junctions of thin graphite flake (Venugopal et al., 2013). Many lithographic techniques in which micro/nanofabrication are possible (Stevenson and Gundlach, 1986).

1.1.1.1.The Photolithography

Photolithography is the most widespread method used for nanofabrication. In the photolithography, photomasks are used to transfer patterns to the photoresist structure and ultraviolet (UV) rays are exposed on this photomask (Pimpin and Srituravanich, 2012). Traditional photomasks are applied by placing metal patterns on molten quartz plates or glasses. In proximity printing and contact printing photolithography, these photomasks are used for transferring the pattern (Kwon et al., 2011). A photomask with a pattern is placed on the photoresist. When the photoresist is exposed to ultraviolet (UV) light, the patterns on the photomask are transferred to the photoresist. Photolithography consists of three modes (See Figure 1). Contact printing and proximity printing photolithography have simplicity that provides high-efficiency products. However, due to the damage to the surfaces of the photomasks during their contact with the photoresist, their usage period is short-term. In addition, since the production of photolithography technique using UV light is limited to the wavelength of the light, nano-scale production cannot be done. On the other hand, the patterned photomasks used for projection printing can be reduced in volume with the help of optical image projection. Photomasks have a smaller line width, making photomasks less sensitive. However, projection printing photolithography type requires a high-quality optical image system and precise process steps (Kim et al., 2007). Briefly, a general photolithography process consists of photomask production, photoresist deposition via spin coating, pre-curing, UV exposure, development, post-curing. Connections between components are indispensable when multilayer photolithography is required. Some patterns need to be made on hundreds of layers by repeating the photolithography steps. Often the photoresist pattern is produced specifically for each layer; this indicates that a large number of photomasks is required for a device production. In summary, the development and practical use of

photolithography is a costly situation that brings some technical and industrial problems.

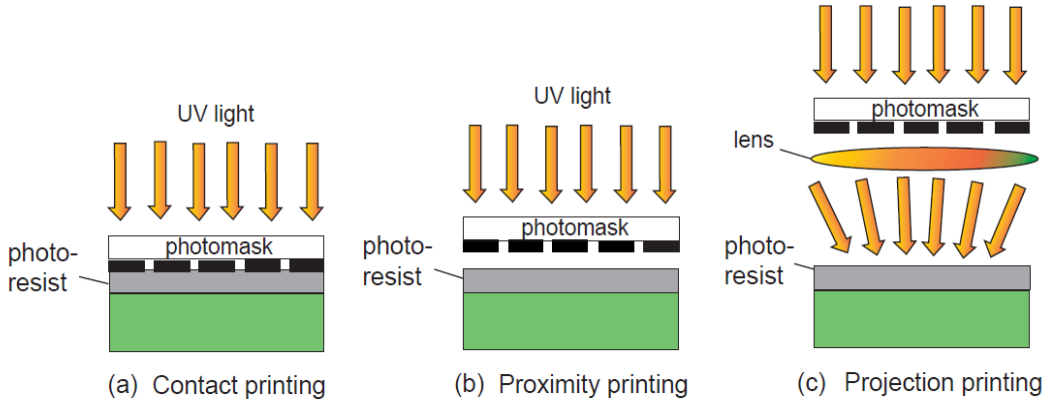

Figure 1. Methods of photolithography (Source: Pimpin and Srituravanich, 2012).

1.1.1.2. X-ray Lithography

This method is a variation of photolithography. The only difference here is that X-rays are used instead of UV as the light source. Since the direct writing or molding is not possible in this method, a mask must be used. X-ray lithography is used for building block integrated microfluidic structures. This technique is known to have applications in genetics and miniaturized instruments such as microchips and microelectrophoresis instruments (Ford et al., 1999).

1.1.1.3. Electron Beam Lithography (EBL)

Another conventional nanopatterning technique is electron beam lithography (EBL). This method is used for the production of patterns on the nanoscale. The EBL technique is a mask-free technique and was first developed for the production of integrated circuits. The biggest advantage of this technique is the use of electrons as the patterning source (Yuce et al., 2017). Therefore, the resolution limitations caused by the light wavelength in photolithography are eliminated (Pfeiffer, 2010). Basically, in the EBL technique, the structures with the desired geometry are written directly on the polymer resist with the focused electron beam with the lenses (See Figure 2). If the resist is positive, the areas exposed to the EBL treatment are selectively removed from the surface by breaking the polymer backbone bonds. If it is a negative resist, the areas

exposed to the EBL process are cross-linked and their removal is prevented. Generally, polymethyl methacrylate (PMMA) is used as the positive resist and hydrogen silsesquioxane (HSQ) is used as the negative resist. Resolutions below 10 nm can be easily obtained in this method (Tseng et al., 2003). On the other hand, in addition to the high costs of EBL systems, mass production is required due to low transaction volumes. Therefore, it is not suitable for technological, industrial applications. Today, it is mostly used in small-scale laboratory research.

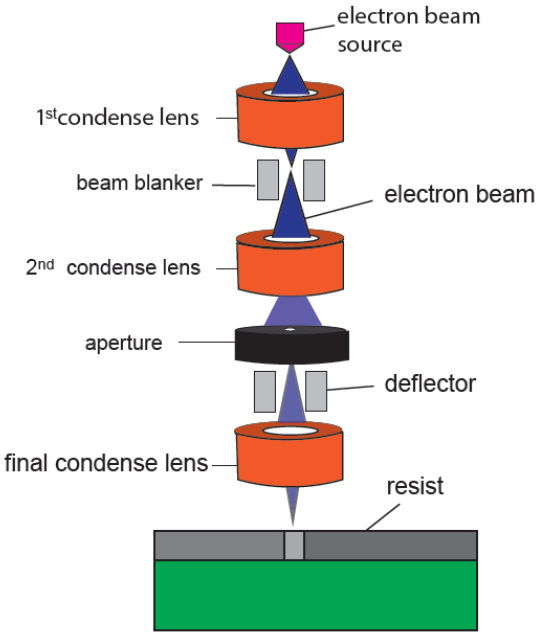

Figure 2. Schematic illustration of electron beam lithography (Source: Pimpin and Srituravanich, 2012).

1.1.1.4. Nanoimprint Lithography

Nanoimprint lithography is used to efficiently produce high-resolution nano-patterns on surfaces. It is based on the principle of printing molds containing topographic patterns on the surface with a thermo-mechanical or UV curing process. It is a very effective method for transferring the patterns to different surfaces and large surface areas with nanometer resolution (Guo, 2007). The most important advantage of this method; once the mold is prepared, it can be simply applied on different surfaces and used repeatedly. Therefore, the process is economical and the production volume is high. Therefore, the method has attracted attention in the semiconductor industry. It is envisaged that the method will be used in chip production and different materials other than semiconductors in the future. On the other hand, the high resolution and

quality mold are required for the method that can only be prepared with EBL. In addition, a device infrastructure with the ability to apply controlled pressure is required for patterning large areas. This increases the infrastructure and process costs and reduces the accessibility of the method.

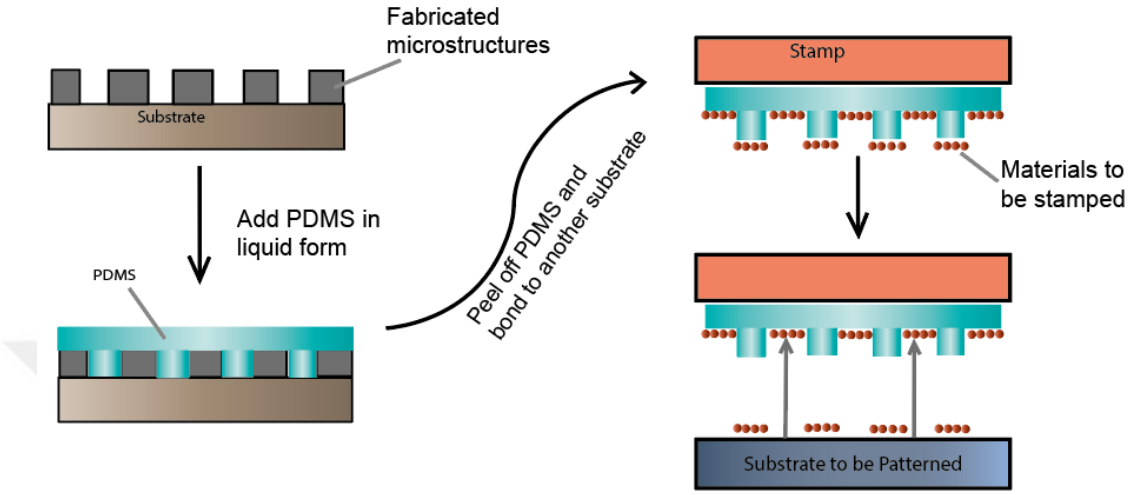

Figure 3. Nanoimprint Lithography molecule transfer process (Source: Pimpin and Srituravanich, 2012).

1.1.1.5. Scanning Probe Lithography (SPL)

It is one of the techniques based on direct writing of patterns that do not require masks or patterns. Scanning probe lithography (SPL) is a technique based on the use of physical microscope probes such as Atomic Force Microscopy (AFM) and Scanning Tunneling Microscopy (STM) for patterning. In this method, molecules at the ATM or STM tip are transferred through a liquid onto the sample surface (Ginger, Zhang and Mirkin, 2004). The molecules that will be patterned on the surface and located at the tip of the needle can be used as ink, and the surface to be patterned can be used as paper (See Figure 4). The resolution of the patterns decreases down to 5 nm with this technique, and at the same time, it is possible to display patterns with an ATM or STM. It has the advantages of being able to achieve high resolutions, covering both basic production methods from bottom-top and top-bottom depending on the mechanism used, and providing high pattern control. For this reason, it is a very suitable method for scientific studies and research (Ginger, Zhang and Mirkin, 2004). Despite these advantages, the SPL process requires a serious infrastructure and experience.

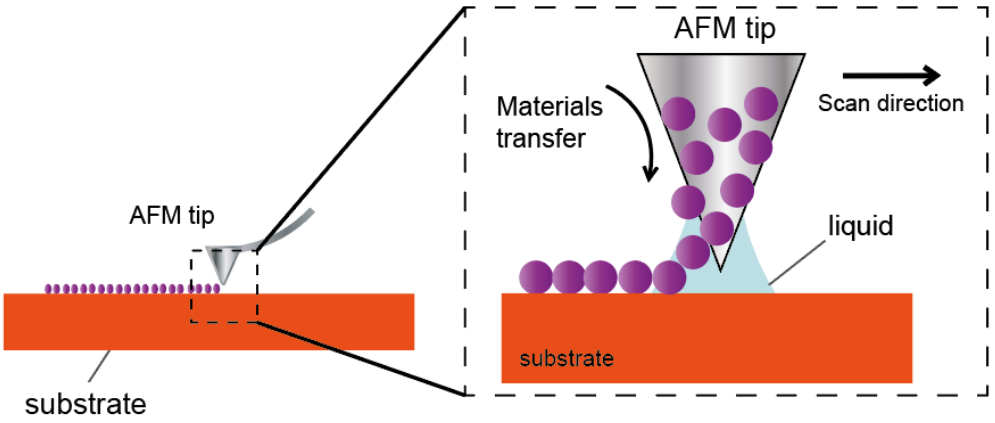

Figure 4. Schematic illustration of Scanning Probe Nanolithography.

1.1.1.6. Electrohydrodynamic Jet Printing (EHD)

Another important technique for the direct formation of patterns is jet printing techniques. It has features such as simplicity, low cost, compatibility with flexible surfaces, ability to form sensitive and multi-molecule-nanocrystalline arrays, and efficient use of materials (de Gans, Duineveld and Schubert, 2004). In this way, jet printing techniques are very promising for patterning surfaces for applications such as microcantilever sensors (Pikul et al., 2011), MEMS resonant sensors (Corbin et al., 2013), thin-film solar cells (Yin et al., 2010), flexible display (Jang, 2006). On the other hand, the smallest line width or dot diameter is between 10-20 µm in patterns that can be reproduced reproducibly with conventional ink-jet printing systems. In the electrohydrodynamic jet printing (EHD) (Park et al., 2007) method, an alternative direct patterning method developed by Rogers et al. that demonstrated pattern fabrication from submicron to 100 nm (Park et al., 2008) can be produced. This technique is based on the writing of polymer-based inks from small aperture nozzles directly on the surface by the effect of an electric field. However, in this method, the pattern resolution is highly dependent on the tip hole, and these small holes can only be provided by highly brittle borosilicate tips produced by the drawing method.

1.2. Nanofibers

The nanofibers produced by the electrohydrodynamic method were used as a tool like a mask in this thesis. In this context, properties, applications and frequently used production methods of nanofibers will be explained in this section.

Nanofibers are defined as extremely fine fibers with diameters in the nanometer range. Fibers obtained from polymer solution and polymer melt in very small sizes, that is, in nanometer diameter sizes, are called nanofibers (Ramakrishna, 2005). Today, nanofibers can be produced from polymer and ceramic materials with different production methods.

Due to the decrease of fiber diameter from micrometers to the nanometer level, nanofibers with large surface areas and improved physical, chemical, and biological properties are obtained. Because of their relatively small fiber diameters, nanofibers with fewer structural defects on their surfaces exhibit a better mechanical performance than conventional fibers. Particularly, their small dimensions cause the expansion of specific surface areas by increasing the nanofibers' surface area/volume ratio. These enlarged surface areas give the ability to bind functional groups, ions, and various nano-level particles to nanofibers (Goddard et al., 2012). They also show high bio-activity, electro-activity, and conductivity due to their small diameters (Buer, Ugbolue and Warner, 2001).

In recent years, nanofibers with high molecular orientation have the potential to improve existing technology and be used in different fields due to their remarkable micro and nanostructural properties (Sunar and Hascicek, 2017). Nanofibers have large surface areas, high porosity structures, a mechanically durable but flexible structure, and conductive nature causing an increase in their usage areas (Sunar and Hascicek, 2017; Hagewood, 2004). Nanofibers are often preferred especially in tissue engineering (Vasita and Katti, 2006), wound dressings (Sylvester, Amini and Tan, 2020), oil-water separation (Sarbatly et al., 2016), filtration systems (Graham et al., 2002), drug delivery (Sharifi et al., 2016), optical sensors (Wang et al., 2002) and the construction of electrodes (Zhang et al., 2016), which are the main components of batteries. The production technology of nanofibers using polymeric materials is quite different from the production of microfibers. The production technology of nanofibers has a very rapid development process with the gaining importance of nanomaterials in

recent years. Nanofibers, which can be produced by drawing, melt blowing, phase separation, and electrospinning methods, are generally produced using the electrospinning method due to the various advantages (Barnes et al., 2007).

1.2.1. Nanofiber production methods

Polymeric nanofibers can be processed by many techniques such as the drawing method, phase separation, melt sputtering, and electrospinning, which are briefly reviewed in this section (Ramakrishna, 2005).

1.2.1.1. Drawing Method

The spinning process is similar to the dry spinning method in the fiber industry. Single and long nanofibers can be obtained with this technique. A typical spinning process for nanofiber production requires a SiO_2 surface, a micropipette, and a micromanipulator (See Figure 5). However, this technique is a laboratory-scale technique in which nanofibers are produced one by one (Ramakrishra, 2005). In this process, a micropipette with a radius of a few micrometers is dipped into the polymer droplet with the help of a micromanipulator. The micropipette is then pulled from the droplet at a speed of about 10^{-4} m/s and the fibers are collected on a surface. The withdrawal of nanofibers is repeated several times on each droplet. The viscosity of the substance at the surface of the droplet increases with evaporation. Therefore, nanofiber production can be carried out by using viscoelastic materials that are cohesive enough to carry the stresses formed during drawing and can undergo strong deformations in the drawing of a fiber (Ramakrishra, 2005). Fiber diameters from 2 to 100 nm to several micrometers and lengths from 10 mm to several centimeters can be achieved with this technique. The quality of the nanofiber depends on the material composition, the draw rate, and the evaporation rate of the solvent.

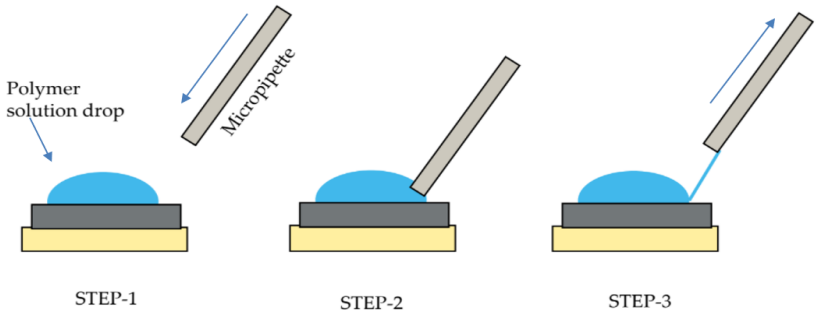

Figure 5. There are three steps in this technique: (a) applying a millimeter drop of polymer solution to the substrate material, (b) micropipette then moving towards the edge of the drop, and (c) contacting and back-moving (Source: Garg, Rath and Goyal, 2015).

1.2.1.2.Phase separation method

In phase separation, a polymer is first mixed with a solvent before gelling. The main mechanism in this process is the separation of phases resulting from physical incompatibility. In this method, a small amount of homogenized polymer solution is poured into a suitable Teflon container. The resulting gelation temperature depends on the concentration of the polymer in the solution. In the final step, the gel is removed from the container and dried using the freeze-drying method (Garg, Rath and Goyal, 2015).

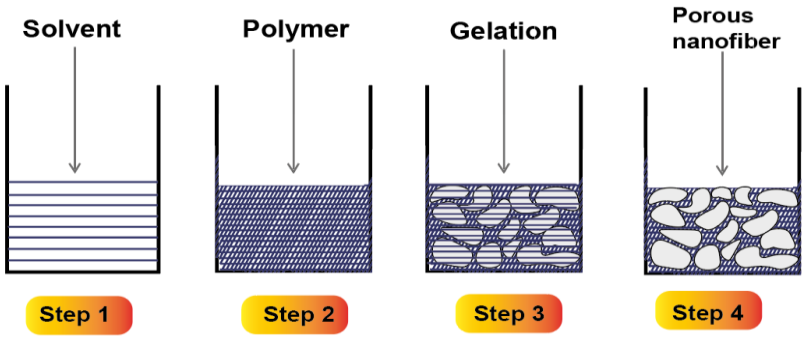

Figure 6. Schematic illustration of phase separation method (Source: Garg, Rath and Goyal, 2015).

1.2.1.3.Melt Blown (MB) Technique

The melt blowing (MB) method is widely used in the production of small diameter fiber recently. Fiber production is melted by blowing hot air at a high flow rate as the polymers come out of the mold. At the same time, fibers are obtained by thinning the polymer with cold air applied from the outside (Fedorava, 2007).

A typical melt-blown (MB) process includes the following components: extruder, metering pumps, die assembly, web formation, and winding. First, polymer pellets or granules are melted in the extruder and fed into the MB die. High-velocity streams of hot air reduce polymer flows to form microfibers. It attracts surrounding air, which cools and solidifies the fibers, and creates a self-adhesive non-woven mesh. Melt-blown meshes ranged from smooth surface texture, high surface area, fiber diameter from 0.5 to 30 m.

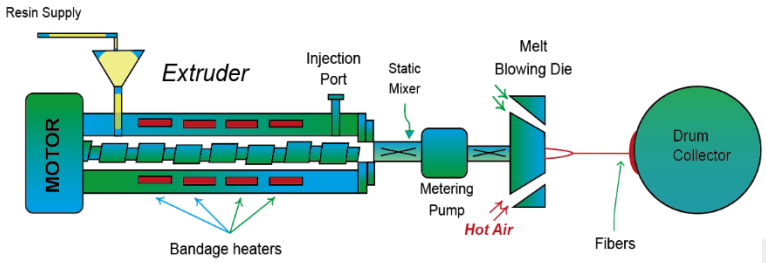

Figure 7. A typical melt-blown process diagram.

1.2.1.4.Electrospinning method

The electrospinning system generally consists of four basic pieces of equipment: voltage source, suitable polymer solution, polymer solution feeder, collector. The polymer is pushed into the needle at the tip of the syringe in a controlled manner with the help of a syringe pump. At this time, by applying voltage, the polymer droplet hanging on the needle tip becomes charged with electricity and the induced charge is evenly distributed on the surface of the droplet (Sigmund et al., 2006). Thus, if the stretched droplet achieves high molecular cohesion sufficiently, it forms a charged liquid jet without flow fragmentation. This jet is thinned by the spin action causing the production of nanofibers. The forces placed on the droplet coming out of the needle tip; gravity, viscosity, surface tension, and electrical tension balance each other to form the structure known as the Taylor cone at the needle tip (Taylor, 1969). After the Taylor cone is formed, at a critical voltage value, the electrical attraction

force dominates the surface tension of the liquid and a polymer jet is formed from the cone tip to the conductive collector located opposite the cone (See Figure 8) (Larrondo and St. John Manley, 1981). If the jet is stable enough, polymer fibers with diameters ranging from micrometer to 50 nm and below can be produced on the collector by bending and stretching of the jet as it moves towards the collector (Greiner and Wendorff, 2007). Nanofiber production is carried out in two groups, laboratory scale, and industrial application. Nanofiber production can be performed both on a laboratory scale and industrially with the electrospinning technique which is known as the newest and most advantageous nanofiber production technique. (Burger, Hsiao and Chu, 2006).

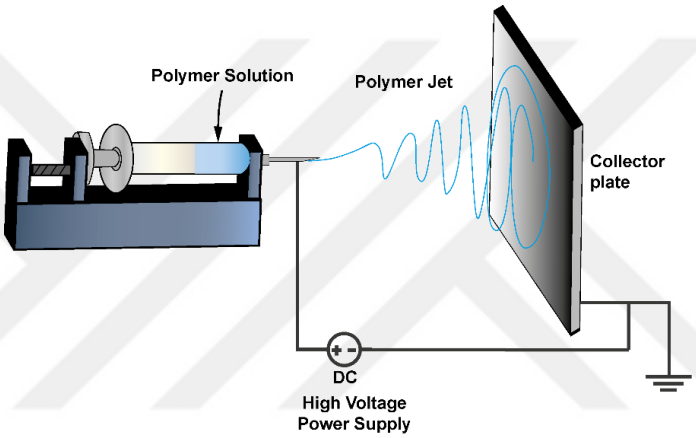

Figure 8. A conventional electrospinning process (far-field electrospinning).

1.3. Electrohydrodynamic Method

In the nanolithography technique produced in this thesis, the patterning of the desired output by positioning the nanofibers is achieved by the electrohydrodynamic method. Therefore, in this section, the electrohydrodynamic method used for the production of nanofibers in controlled diameters/lengths and positioning of nanofibers will be explained.

The production of nanometer-sized structures is important for current and emerging technologies. Today, it can produce fiber structures in sizes and shapes below 100 nm with lithographic techniques. However, the high costs of the advanced lithographic equipment used to manufacture these structures preclude their use in engineering applications or scientific research. Additive manufacturing approaches, which allow working with material directly on a substrate, provide a solution to these

challenges. Unfortunately, the resolution problems arise in inkjet printing technology, which is a low-cost and easy method for additive manufacturing. The electrohydrodynamic printing method offers a solution to the limited resolution of conventional inkjet printer systems by using different methods (Park et al., 2007).

Extremely high-pressure levels are required to overcome capillary forces in thermal and piezoelectric printers. Therefore, the method of extracting liquids from small nozzles can be used. Pushing viscous liquids through a thin capillary is not an easy method, but it is relatively easy to pull liquids from the nozzle through the use of applied electric fields (Basaran, 2002). In the electrohydrodynamic printing technique, a voltage is applied between the nozzle and the opposing conductive support to initiate ink flow from the nozzle via electrohydrodynamics. Typically, a back pressure feed (syringe pump, compressor, etc.) delivers ink to the tips of nozzles as small as ~1 μm inside diameters. These nozzles are typically fabricated by pulling glass pipettes and coating them with a thin metal layer (e.g.Au). The electric field causes mobile ions in the ink to accumulate near the surface of the droplet at the tip of the pipette. The coulombic repulsion between these ions transforms the droplet into a conical shape known as a Taylor cone seen in Figure 9 (Geoffrey Ingram Taylor, 1964). In high electric fields, droplets or polymer jet begin to emerge from the cone when the electrostatic forces overcome the surface tension. Although the charge carriers are required, experiments show that printing is possible even with liquids with low electrical conductivity (10^{-13} to 10^{-3} Sm^{-1}) (Jayasinghe and Edirisinghe, 2004). It becomes possible to pattern the ink material on the surface by changing the position of the substrate simultaneously.

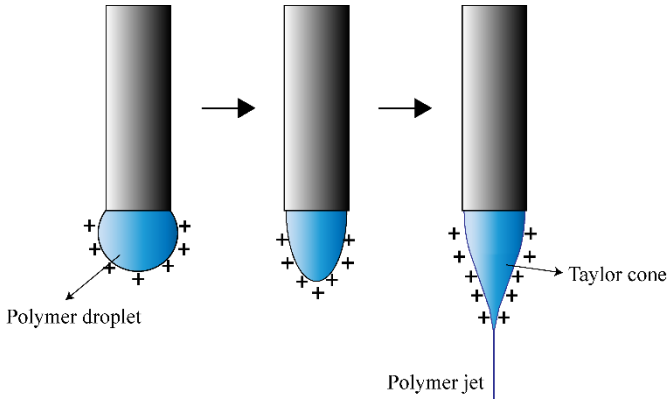

Figure 9. Schematic illustration showing Taylor cone formation and polymer jet initiation from Taylor cone tip under an increasing potential difference.

Electrohydrodynamic processes are simple and inexpensive methods that do not require high temperatures and do not use organic solvents. The electrohydrodynamic (EHD) printing is a process that can achieve three types of printing modes with a same setup (See Figure 10a), called as E-jet printing, electrospinning, and electrospraying (See Figure 10b).

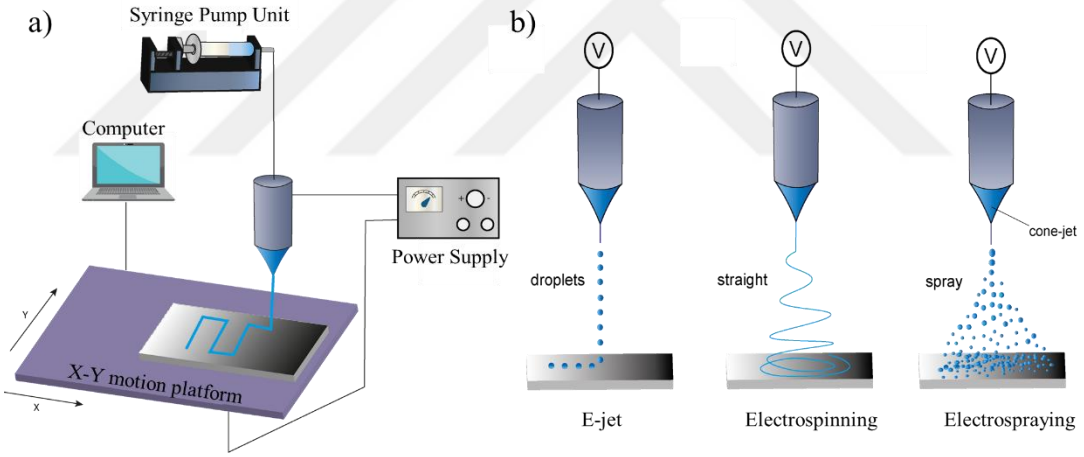

Figure 10. Schematic illustration of (a) the electrohydrodynamic (EHD) printing setup and (b) printing modes.

Basic EHD systems consist of a high voltage power supply, a syringe pump unit, and a grounded collector (Bhushani and Anandharamakrishnan, 2014). In principle, electrospinning and electrospraying are processes in which a polymer solution can be elongated or sputtered by the application of a high potential electric field to obtain fibers or particles. In EHD printing systems, hydrodynamic collector units are integrated into these processes at close distances, and printing is carried out with the created fibers or particles.

The difference between electrospinning and electrospraying methods is based on the viscosity and concentration of the polymer solution (Niu et al., 2011). When the solution viscosity and concentration are high, the polymer jet emerging as a Taylor cone stabilizes and elongates to form fibers. When the solution viscosity and concentration are low, the jet is not stabilized and fine droplets are formed (Bhushani and Anandharamakrishnan, 2014).

Electrohydrodynamic direct writing printing is a method that combines electrospinning and 3D printing. The electrohydrodynamic method is a method that enables the production of nanofibers of homogeneous diameter and various compositions under a certain electric field using a polymer solution and patterning of the produced nanofibers on various substrates. In this method, fiber production is carried out by uniaxial elongation of the viscoelastic jet in the polymer solution under the influence of electrical forces. Nanofibers produced by the electrohydrodynamic method could be used in tissue engineering (Castilho et al., 2017), drug delivery systems (Minden-Birkenmaier et al., 2017), sensors (Chen et al., 2013), field-effect transistors (Wang et al., 2018), transparent electrode production (Kim et al., 2018; Wang et al., 2017), lithium-ion batteries (Liu et al., 2017; Chen et al., 2017), and supercapacitors (Lu et al., 2017). In addition, the fibers produced by the electrohydrodynamic method create biomimetic structures in direct writing and a lab-on-a-chip technology (Agarwal et al., 2008; Agarwal et al., 2009), and form layers for nanochannel production (Yarin et al., 2007; Feng et al., 2010) and conductive nanofibers are also used in field-effect transistors (Min et al. 2013).

1.3.1. Advantages of Electrohydrodynamic Method

The main reasons for using the electrohydrodynamic method are that it is fast, suitable for mass production, and repeatable (Dincer et al., 2016). The electrohydrodynamic method allows the production of nanofibers using different polymers, relatively less energy, and less raw material compared to other methods (Dincer et al., 2016). It is possible to produce nanofibers between 3 nm-1μm with different polymers by the electrohydrodynamic method (Huang et al., 2003). In the electrohydrodynamic method, which is the most common method in nanofiber

production, uninterrupted nanofibers and nanotubes could be produced with diameters ranging from 10 to 100 nm (Torres et al., 2019).

The nanofibers can be produced in long lengths, with solid and hollow interior structures and homogeneous diameters (Dan and Xia, 2004).

1.3.2. Designs and Applications of Electrohydrodynamic Method

The production of the electrospinning method is shaped according to the characteristics of the desired product and there are different types used in the literature. There are four different types of electro-spinning methods used in the literature.

- conventional electrospinning for the fabrication of non-woven and nanofibers,
- electrospinning with fiber insertion with auxiliary electrode or dynamic collector,
- near-field electrospinning with the positioning capability of electromagnetic exposure,
- mechano electrospinning for positioning nanofibers and studying their morphology in one step.

The first of these is the traditional electrospinning technique used for the pattern-free and random fabrication of nanofibers. In this method, a polymer jet is formed irregularly. However, the purpose of using the electrospinning method has evolved. To use nanofibers in electronic systems, a high degree of positioning of the fibers is required rather than disordered structures. In this context, first of all, changes have occurred in the design of the system and the composition of the solution. Firstly, by using a dynamic collector, it is possible to pattern nanofibers, although not in high resolution. These methods are called electrohydrodynamic processes. The electrohydrodynamic method combines the dynamic 3D printing method and the electrospinning method to position the fibers at a high degree.

One of the first examples of this method is patterning, in which the rotating disc collector is used as a collecting base in the system. The distance between the nanofibers could be controlled relatively (Theron et al., 2001). Another method is the electrohydrodynamic method with support electrodes. In this method, polymer, ceramic, and polymer/ceramic composite nanostructures are patterned between

conductive electrodes standing parallel to each other (Li et al., 2003). However, electrospinning with auxiliary electrodes or dynamic mechanical collectors only aligns the fibers. These methods cannot control the positioning of a single fiber precisely. The fibers produced in these methods cannot be used in electronic applications due to irregular alignment. It is important to manipulate a single fiber to fabricate structures and devices at the micro/nanoscale (Teo and Ramakrisha, 2006). In recent studies, more detailed microstructures are produced by improving the control in the positioning and morphology of the fibers (Chang et al. 2008)

In particular, the electrohydrodynamic method has many advantages over other internal pressure-based inkjet printing techniques. Positioning a single fiber is one of the most challenging tasks in electrospinning. The distance between the needle and the collector should be decreased to prevent the bending of the fiber that occurs when the collected nanofiber contacts the collector. If the distance is less than 3 cm, regular patterns of fibers can be obtained without the need for an auxiliary electrode. The electrohydrodynamic method has started to take its place especially in the production of nanofibers with this feature. Kameoka et al. developed the scanning type electrohydrodynamic method, which reduces the type and collector distance to 0.5-1 cm and allows the use of polymeric nanofibers (Kameoka et al., 2003). However, the positioning of nanofibers in this method is insufficient. In the electrohydrodynamic method developed by Sun et al., the distance between the type and the collector was further reduced to less than 1 mm, and the atomic force microscope type was used as the type. Polymer jet was produced with the drop obtained by dipping type into the polymer solution (Sun et al., 2006). However, the tungsten electrode with a type diameter of 25 µm collected only a very small volume of solution, causing the solidification of the solution. The polymer solution on the tungsten tip was consumed as the process progressed, so the limited area could be covered with nanofiber. Gupta et al. used a spray hose connected to a solution reservoir to solve the problem of solution collection in a limited volume (Gupta et al. 2007). In addition, to increase the positionability of the fibers, a needle tip was placed on the collector to serve as a guide electrode. In another electrohydrodynamic method developed by Chang et al, a syringe needle is used to continuously feed the polymer solution, just like the conventional electrospinning method. Then, by applying 600 V voltage, the polymer solution was passed through the tungsten type (1 µm in diameter) and 100 nm thickness-108 m long

nanofiber was produced. It has also been shown that with this method, the spinning process can progress continuously by feeding the polymer solution from the spray nozzle for 15 minutes (Chang et al., 2008). It is very important to align semiconductor nanofibers in the desired size, number, and precisely and to print them at high speed and in large areas for electronic device applications. Min et al. designed a high-speed nanofiber printer to print large-area organic semiconductor nanofiber arrays by the direct electrohydrodynamic method. The maximum field-effect mobility of 9.7 cm2/V. s at very low contact resistance (<5.530 Ω) was achieved with this printer, even with nano-channel transistors consisting of single semiconductor nanofibers. Complementary inverter circuit arrays containing well-aligned p-type and n-type organic semiconductor nanofibers have also been fabricated (Min et al., 2013). Thus, a simple, reliable method has been developed to fabricate large-area nano electronic devices that perform extremely fast nanolithography by directly writing semiconductor nanoarrays. The purpose of the above-mentioned studies is to use nanofibers, which are directly printed and used in electronic device applications.

1.3.3. Parameters Affecting Electrohydrodynamic Printing

The electrohydrodynamic printing technique has a multidisciplinary working principle that combines many disciplines such as fluid mechanics, polymer chemistry, physics, and electricity. The presence of many parameters affecting the process makes the controllability of the system very difficult (Rosic et al., 2012). However, by well understanding and optimizing the effects of the parameters classified in Table 1 on fiber morphology, it is possible to obtain smooth nanofibers with the desired morphology.

In an ideal electrohydrodynamic printing process compatible and controllable fiber diameters, and continuous nanofiber formation should be ensured (Burger, Hsiao and Chu, 2006).

Table 1. Parameters affecting the electrohydrodynamic printing process (Source: Schiffman and Schauer, 2008).

Solution Parameters	***Process Parameters***	***Environmental Parameters***
• Solution viscosity • Molecular weight of polymer • Surface tension of the solution • Solution conductivity	• Applied voltage • Distance between needle and collector • Solution flow rate • Type of Collecting Pad • Needle Tip (Nozzle) Diameter • Collector of Speed	• Temperature • Humidity • Air flow rate

1.3.3.1.Solution Parameters

Solution viscosity

The viscosity of the solution used in the electrohydrodynamic method has important effects on the fiber dimensions, and the viscosity must be optimized to form nanofibers in the desired morphology. A low polymer solution viscosity means that the polymer solution has low chain entanglement. Insufficient chain entanglement causes the surface tension forces to dominate in the polymer jet. This prevents continuous polymer jet formation and causing the beaded structure to be used more frequently on the fiber surfaces formed. When the solution viscosity is increased, the formation of the beaded structure is prevented by ensuring the continuity of the polymer jet (Fong, Chun and Reneker, 1999). In addition, this increase in solution viscosity prevents whipping instability of the jet and shortens the path it will take. Thus, less elongation of the solution causes an increase in fiber diameters (Barnes et al., 2007). When the solution viscosity is too high, the electrostatic forces on the droplet cannot overcome the surface tension, making it difficult to form the polymer jet and pump the drop formed at the needle tip. In this process, the droplet, which cannot reach the collector, dries and clogges at the capillary tip (Fong, Chun and Reneker, 1999).

Molecular weight of the polymer

There is a linear relationship between the molecular weight of a polymer and the chain lengths, and an increase in the molecular weight of the polymer means an increase in the chain lengths. Polymer chains with increasing length tangle more easily with each other. This leads to an increase in chain entanglement and thus an increase in inter-chain interactions. These entanglements between the polymer chains prevent the continuity and dispersion of the polymer jet during the movement of the solution from the needle tip to the collector plate in the electrohydrodynamic method. Therefore, polymers with very low molecular weights are not suitable for fiber formation. In addition, as the molecular weight of the polymer increases, the formation of bead-like structure in the fiber structure decreases and the fiber diameter increases (Haghi and Akbari, 2007; Tan et al., 2005).

Surface tension of the solution

In order to initiate polymer jet, the charged solution must exceed its surface tension. Surface tension is an effective parameter for reducing the surface area per unit mass of a liquid. Surface tension force can also cause bead formation during spinning. When there is a high concentration of free solvent molecules, the solvent molecules have a great affinity for coalescence and take a rounded shape due to surface tension. High viscosity means that there is a strong interaction between the solvent and polymer molecules. Thus, when the solution stretches under the influence of loads, the solvent molecules tend to diffuse over the branched polymer molecules and the tendency of the solvent molecules to come together under the influence of surface tension decrease (Burger, Hsiao and Chu, 2006).

Solution conductivity

Solution conductivity is defined as the ability of the solution to carry an electrical current. A polymeric solution must have a certain conductivity value to be

used in the electrohydrodynamic method. If the polymer solution does not have sufficient conductivity, it can be used in the electrohydrodynamic method by increasing the conductivity of the solution and adding some salt or polyelectrolyte. When the load-carrying capacity of the polymer jet increases, the polymer jet is exposed to greater tensile forces in the electric field. Thus, fiber diameters are decreased (Sill and Von Recum, 2008). However, if the conductivity reaches very high values, the polymer jet can become flexural instability within the distance between tip and collector. Thus, in the fiber structure are occurred large diameter changes (Hayati, Bailey and Tadros, 1987).

1.3.3.2.Process Parameters

Applied voltage

The voltage applied to the solution is another important parameter in the electrohydrodynamic process. Fiber formation is observed only when a certain threshold value is exceeded. In the conventional electrohydrodynamic method, it has been observed that the critical voltage value is 6 kV for the formation of the Taylor cone by overcoming the surface tension. It was stated that below this voltage value, the polymer drop could not take the Taylor cone form. Thus, the nanofibers could not be formed (Ramakrishna, 2005). Generally, nanofibers with larger diameters and beaded structure are obtained at minimum voltage values. As the voltage is increased, the polymer jet lengthens and becomes thinner due to the increase in electrical forces affecting the polymer solution. This causes a decrease in fiber diameters (Ramakrishna, 2005). However, the increase in tension provides thinning of the fibers up to a certain point. Exceeding the optimum voltage value leads to the thickening of the fibers again (Sill and Von Recum, 2008). Above the optimum voltage value, the polymer jet becomes unstable, forming multiple jets. Increasing the velocity of the formed polymer jet delays the forces on the jet to repel each other and create a radial torque. The whipping instability is started late due to this delay. The jet could not find enough time and way to stretch and thin in the air, thus increasing the fiber diameters and bead-like structure formation on the surfaces (Rosic et al., 2012).

Distance between needle and collector

The distance between the needle tip and the collector is another important variable that affects fiber morphology. At this distance, the solvent is removed from the formed fiber. The fiber solidifies until it reaches the collector. As this distance increases, the fineness of the fiber increases due to the increase in the distance followed by the jet, and the fibers are collected in a dry state. The longer the distance between the needle tip and the collector, the longer it takes for the solvent to evaporate. If the distance is too low, the fibers are collected as wet, this causes beaded structures. As a result of their study, Buchko et al have observed the formation of a bead-like structure depending on the electric field strength located between the nozzle and the collector when the distance is very small. The decrease in the distance between the nozzle and the substrate has a similar effect with the increase in the applied voltage (Ramakrishna, 2005).

Solution flow rate

The rate of the polymer solution to the collector is another important parameter that affects fiber diameter and morphology. Thus, the appropriate flow rate is required to form a stable Taylor cone. If the flow rate is lower than necessary, the polymer solution attracted by the electrical forces at the needle tip could not be fed to the needle tip at the same speed, resulting in the formation of a discontinuous Taylor cone (Sill and Von Recum, 2008). Thicker fiber diameters are observed due to the increase in the drop mass formed at the needle tip with the increase of the feed rate. When the flow rate exceeds the critical value, the drying time of the jet is insufficient for the evaporation of the solvent from the needle tip to the collector, as well as bead formation on the fiber surfaces (Yuan et al., 2004). As the nanofibers reach the collector, it is expected that the solvents in the fiber structure will evaporate and leave the fibers. Otherwise, due to the solvent content of the fibers, fusions and adhesions occur at the points where they come into contact with each other while drying on the collector. It is observed that there is a flattening in the structure of the fiber with the effect of the electric field and the fiber takes on a strip-like appearance (Bhardwaj and Kundu, 2010).

Speed of collector

Speed of collector is an important parameter in patterning micro/nanostructures in the electrohydrodynamic method. Nanofibers can be positioned on the substrate in different patterns by controlling the collector speed. Collector speed affects the nanofiber structures and movement of the polymer jet. When the collector speed is lower than the ejection speed of the jet, oscillating motion is observed in the fibers. When the collector speed is increased, the density and width of the pattern created with nanofibers can be reduced by the drag force from the collector (He et al., 2013). The optimum collector speed should be adjusted according to the determined pattern and fiber structure.

Type of Collecting Pad

The type of guide pad is also important during the process, and either the pads must be conductive or a guide electrode must be used to generate the electric field. Therefore, conductive materials such as aluminum foil are used as a collecting base. If a non-conductive substrate is used, less fiber deposition occurs on the collector.

Needle Tip (Nozzle) Diameter

Studies with different needle tip diameters show the effect of needle tips on fiber diameters and electric fields. Hartman et al. examined the effect of nozzle diameter on the polymer cone structure formed at the needle tip and patterning, and it was concluded that the current depends on the nozzle diameter (Hartman et al., 1999). In addition, as the needle tip diameter decreases, the fiber diameter and bead formation in the fiber structure decrease. In addition, it is necessary to reduce the needle diameter for the production of patterns on the nanometer scale with fibers.

1.3.3.3.Environmental Parameters

Atmospheric conditions have a significant effect on the structure of the fiber to be produced. These important conditions can be listed as humidity, pressure, and temperature.

Humidity

Humidity has a direct effect on the surface morphology of nanofibers. In a high humidity environment, a porous fiber structure occurs due to the condensation of water molecules on the fiber. Increasing the amount of moisture causes the size and depth of the pores to increase. Studies show that smoother fibers are obtained in studies performed under 50% humidity. The humidity of the environment also affects the rate at which the solvent evaporates from the fiber during electrohydrodynamic method. The evaporation rate of the solvent is higher in non-humid environment (Ramakrishna, 2005). It has been observed that the obtained polystyrene nanofibers have a smooth structure when the humidity in the environment is lower than 25%. Significant changes were observed in the surface morphology of the fiber with the increase of the humidity to 31-38%. This variation is rounded pores randomly distributed on the fiber surface. In the range of 40-45%, the shape of the pores did not change, but they increased intensively on the fiber surface. The most remarkable increase was observed in nanofibers drawn in the range of 50-59%. The pores increased without leaving any gaps on the fiber surface by the increase in humidity. The pore shape changed from circular to non-uniform structures with the merging of small pores. At 60-72% humidity, there are also non-uniform pores, but they are larger than the pores formed at 50-59% (Ramakrishna, 2005).

Temperature

Since the ambient temperature can change the rheological properties of the polymer solution, it is also very effective in changing the fiber diameter. Especially with the increase in temperature, temperature decreases in solution viscosity. Thus, surface tension facilitates the elongation of the polymer jet. It enables to obtain finer and uniform fibers (Mit-Uppatham, Nithitanakul and Supaphol, 2005). According to Zeng et al., controlling of the electrohydrodynamic method process is easy in summer and difficult in winter. They have observed that the PLLA nanofibers obtained by electrohydrodynamic method at room temperature (25°C) in summer have uniform

diameter distribution. When they adopted the same production conditions to room conditions (7°C) in winter, the nanofibers were not uniform due to the slow solvent evaporation (Zeng et al., 2014).

1.4. Physical Vapor Deposition Methods

In this thesis, first of all, the desired output material (Metals e.g., Au, Ag) is coated on a substrate and then nanofibers are patterned on this coating by electrohydrodynamic method. In this section, Physical vapor deposition methods, which are the methods used for metal deposition on substrates, will be explained.

1.4.1. Magnetron Sputtering Method

The sputtering technique is a physical vapor deposition method based on the principle of physical deposition of atoms detached from a target material by positive ions on the desired substrate. In this method, the vacuum chamber is first put under vacuum with a vacuum pump. An unreacted inert gas such as Argon (Ar) is then used in a controlled manner into the vacuum chamber (Thornton, 1983). As a result of the collision of the Ar atoms with the accelerated electrons under a high electric field, the Ar atoms are ionized. The transitioning of Ar atoms to the positive state moves towards the cathode in the electric field and strikes the target material positioned in front of the positive (+) cathode, causing the target material atoms to break. The process results in the deposition of these atoms, which possess kinetic energy as a result of the collision, on the substrate placed in front of the anode (See Figure 11). According to the target material used, two different types of sputtering operations are carried out as DC and RF voltage. If the target is conductive, for example, to deposit aluminum-doped zinc oxide (AZO) thin films (Turkoglu et al., 2018) or Vanadium oxide (VOx) thin films (Alaboz et al., 2017), a DC Sputter is used (Tavsanoglu, 2009). The RF sputter technique is used to obtain materials from conductive and insulating targets. In the method known as the magnetron sputter technique, a magnetic field is used while trapping electrons close to the target in certain directions to adjust the number of atoms to be grown and to remove atoms from a certain region of the material used as the

target. Thus, Ar atoms ionizing in these regions can detach atoms from the target (Yuce, Aygun and Koklu, 2015; Unlu et al., 2016).

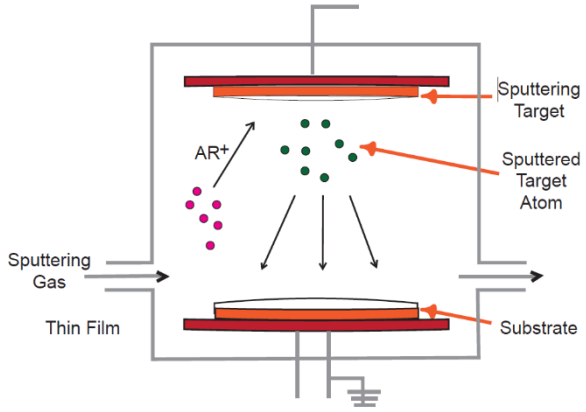

Figure 11. A schematic diagram of the magnetron sputtering method (Source: Bellardita et al., 2019).

1.4.2. *Thermal Evaporation Method*

Thermal evaporation is a technique used to coat a metallic or chemical material layer as a thin film on a metallic or non-metallic (plastic, glass, ceramic) substrate. This technique is the process of coating atom-to-atom or molecule-to-molecule layers on a solid surface at low vacuum. Typically, vacuum processes are used to tune film thicknesses ranging from a few nanometers to thousands of nanometers. Vacuum evaporation generally occurs in the range of $1.33x10^{-5}$ mbar to $1.33x10^{-9}$ mbar. Evaporation of the material occurs inside a tungsten boat. Tungsten metal is selected because it has a good resistivity ($52.8x10^{-9}$ Ω .m) and a high melting point (3380ºC). The temperature is increased to the point required for the evaporation of the source material with the high current flow through the boat. The steam resulting from the evaporation process of the source material is produced in a vacuum and dispersed again in a vacuum. The source material is separated into atoms or groups of atoms (parts of molecules, groups). This vapor diffuses around the vacuum and condenses on the coated substrate. Illustration of thermal evaporation system is shown in Figure 12.

High purity films can be coated with high purity source materials and the source material to be evaporated can be a solid of any shape and purity (Chang, 2001).

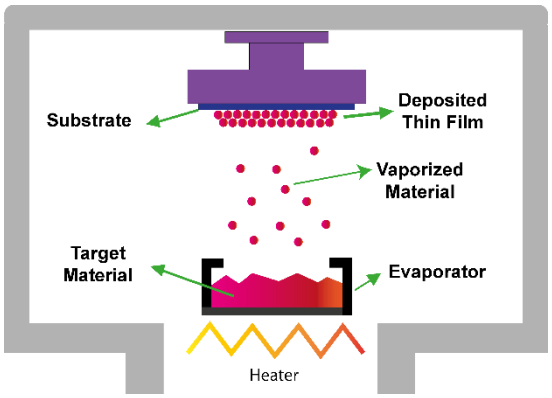

Figure 12. Schematic illustration of Thermal Evaporation Deposition.

1.5. Argon Ion Beam Etching Method

In this section, after patterning on metal coated substrates using EHD method, Argon ion beam etching method used to remove metal on non-fiber-coated area will be explained.

Ion Beam Etching (IBE) is a physical dry etching technique that atoms on the sample surface are removed under vacuum by accelerated Argon ions. It is also a sputtering process that can be used to create a pattern on the surface of the substrate using masks or to pre-clean a substrate. Unlike with sputtering targets, the atoms of the sample are removed by the energy transfer between the sample surface and the accelerated Argon atoms.

In the ion beam etching process, plasma is created in a reaction chamber under high vacuum. Meanwhile, corrosive gases such as Argon are sent to the reaction chamber at certain rates. Gases that are ionized in the plasma gain a certain energy in proportion to the power given to the plasma. Then these ionized gases are directed at certain angles on the sample to be etched. As a result of this process, the ions hitting the sample surface create a chemical reaction or bombard the surface. In this way, the sample material is removed from the sample surface (Chekurov et al., 2009; Koseoglu et al., 2011).

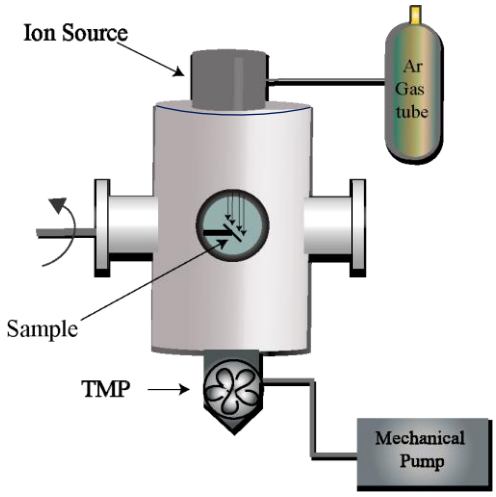

Figure 13. Schematic illustration of Argon Ion Beam Etching Method.

1.6. *Atomic Force Microscopy (AFM)*

In this section, atomic force microscopy, which is used to measure the morphology and dimensions of the fibers before and after the etching process and the obtained metal patterns, will be explained.

Atomic force microscopy can perform topographic imaging, force measurement, and manipulation by probing the surface of the sample with a silicon tip. The tip of less than 10 nm mounted on the silicon cantilever, is usually 80 to 300 microns long. The light from the laser diode has reflected the detector from the back of the cantilever. The detector measures the deviation values of the cantilever with the light reflected on the detector and converts this measurement into an electrical signal. The intensity of this signal is directly proportional to the deviation of the console. The tip position is obtained using the laser diode light reflected by the console on a photodiode display (See Figure 14). During the scanning, the feedback system minimizes the deviation by adjusting the vertical position of the sample. The lateral resolution of the AFM is defined by the tip size and the sensitivity of detecting the spot laser position on the photodiode. The main force between the tip atoms and the sample atoms is an interatomic force called the van der Waals force (Bowen and Hilal, 2009). Depending on the sample-tip distance, three measurement systems are possible: In tapping mode, the cantilever is progress to oscillate up and down at or nearby resonance frequency. In the contact mode, the tip slides very close (a few angstroms) off the surface creating interatomic repulsive force. In the non-contact mode, the

cantilever is held in order from the sample surface to tens to hundreds of angstroms, and interatomic forces create attraction (Garcia and Perez, 2002). In addition to the van der Waals force, other forces also occur. For example, in air measurements, a thin layer of water forms between the tip and the sample surface in a high humidity environment. Capillary forces keep the tip in contact with the sample surface, as it is due to the thin layer of water in the contact mode. In summary, in the absence of an external field, the dominant forces are Van der Waals interactions, short-range repulsive interactions, and long-range adhesion forces, as well as capillary forces and elastic cantilever forces. The distance between tip and sample determines the type of force to be sensed. Tapping mode, is mostly preferred for ambient conditions and liquids. Most samples form a liquid meniscus layer in ambient conditions. Therefore, the probe type must be held close enough to the sample for short-range forces to become detectable. However, sticking the tip to the surface should also be avoided. In such operations, the contact mode presents a major problem. Tapping mode (intermittent or dynamic contact mode) was developed to solve this problem. In recently, tapping mode is widely used AFM mode for ambient conditions or liquids (Zhong et al., 1993). The contact (contact) mode is preferred when atomic-scale images are needed because in this mode the tip is in close contact with the sample and a better lateral resolution can be achieved. Because a strong mechanical interaction occurs between the tip and the sample surface, the contact mode is suitable for hard and relatively flat surfaces, but not for soft samples such as organic or biological objects. In the non-contact system, the tip vibrates (close to the cantilever resonance frequency) near the sample surface at a distance of 10 or 100's Angstrom. Many scanning vibration modes are available, such as non-contact, intermittent contact mode, oscillating technique, half-contact mode, tapping mode, etc. They differ in the distance between the tip and the surface and the feedback control of the tip oscillation. Limited contact with the surface reduces tip wear and surface damage, so this

technique is suitable for any sample from soft to hard in a large variety of sample topography (Eaton and West, 2010).

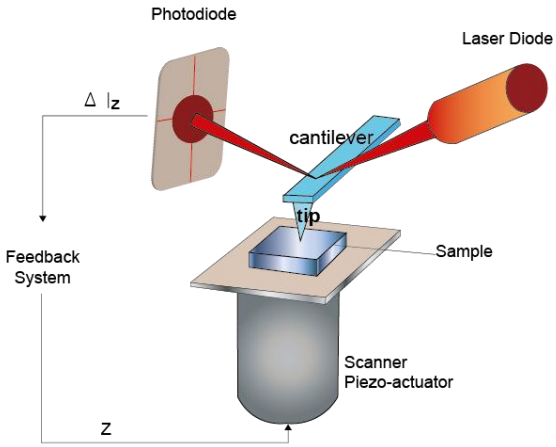

Figure 14. Schematic illustration of AFM working principle.

1.7. *The motivation of this study*

In this thesis, it is aimed to produce micro/nanoscale metal electrodes by patterning with nanofibers written directly on the substrate by electrohydrodynamic method. For this purpose, a system that can produce the desired patterns on the substrate has been established by combining the electrohydrodynamic method and a platform that can move in x-y axes (See Figure 15). The nanofiber layer produced by the electrohydrodynamic method acts as a mask. Metal layer on non-fiber-coated areas is etched by Ar ion beam etching method. Desired metal patterns are produced by removing the polymer on the pattern. The stages in this thesis are summarized in Figure 16. In the previous studies, nanofibers were produced for use, however in this thesis nanofibers were used as a tool for patterning. Thus, an alternative method to the methods used in micro/nanomanufacturing has been developed.

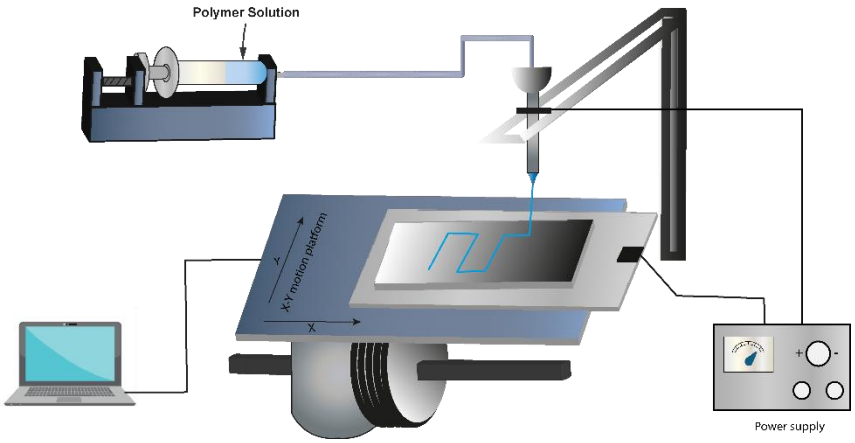

Figure 15. The experimental setup of the electrohydrodynamic method consists of a power source, a syringe pump, and a collector that can be moved in x-y axes by a computer software.

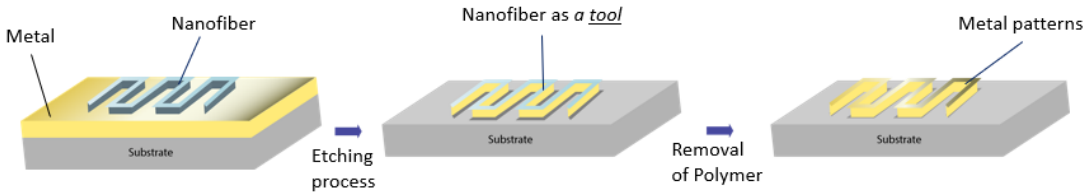

Figure 16. Schematic illustration of three steps in this thesis: patterning with EHD method, Argon ion beam etching, and removal of polymer.

CHAPTER 2: MATERIAL AND METHODS

2.1. System Installation and Pre-Optimization Studies

First of all, the platform that provides the movement of the collector and the software that guides the platform is provided to work with the electro-spinning system. In this regard, the mechanism that enables the x-y platform to work with the software has been installed. The controllers of the x and y motors are connected to the Mach3 board and the x and y servo motors. The circuit board is then connected to the computer via USB. The platform was calibrated as a result of speed tests of x and y motors using Mach3 software. The automatic setting option is used in the Mach3 program. In this way, the actual distance traveled by the motorized platform is measured after selecting an axis and entering a distance. This distance is entered into the program, which automatically suggests the number of steps per unit (SPU) so the calibration process is performed. The SPU of each engine of the studied system was determined as approximately 3846.16.

In the software, by ensuring that the specified speed does not exceed the maximum speed of the motor, speed adjustment can be made with the G-code. G-code is a programming language used for numerical control purposes. It is generally used in computer-aided production to control automatic machine parts.

The electrohydrodynamic method consists of three basic components, which are high voltage source, solution supply unit, and the collector (See Figure 17). The solution feeding unit consists of a syringe with polymer solution in a metallic needle and a syringe pump that feeds the solution towards the needle tip in a constant and controllable manner. In this context, the syringe pump and voltage source, and the elements of the platform are made to work together.

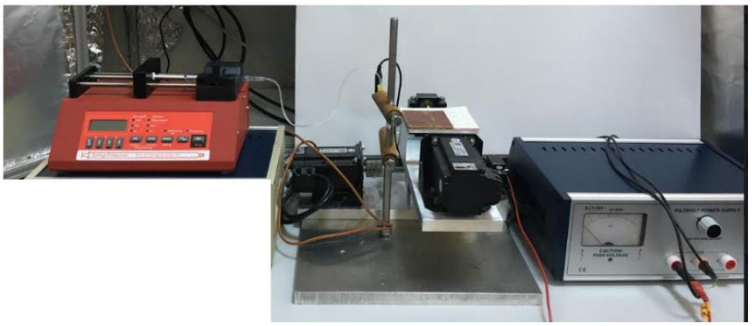

Figure 17. General view of the used electrohydrodynamic method.

2.2. Substrate Preparation

2.2.1. 100 nm Ag Coatings on Si/SiO_2 Substrates

Optimization studies were carried out on SiO_2 substrates with silver coatings. In this regard, SiO_2 is coated with silver in 100 nm thickness by using the physical deposition system (Leybold Univex 300) in the infrastructure of the Research and Application Center for Quantum Technologies (RACQUT). The current applied during evaporation is 68 A and the evaporation rate is 0.7 kA/s. The nano-patterning studies were carried out by drawing flat fibers in a grid structure on silver-coated silicon dioxide substrates with the electrohydrodynamic technique. After the patterning, silver was etched for 5 minutes by reactive ion etching technique so the polymer-coated silver fibers were obtained. The thickness and morphology of the fibers were visualized by scanning electron microscopy (SEM) and atomic force microscopy (AFM).

Figure 18. Photograph of the physical deposition system (PVD) (Leybold Univex 300) in the infrastructure of the Research and Application Center for Quantum Technologies (RACQUT).

2.2.2. 10 nm Cr + 100 nm Au coatings on glass substrates

Electrohydrodynamic method studies were also carried out on chrome and gold-coated substrates by using the parameter values obtained from electrohydrodynamic method studies on 100 nm Ag coated substrates. Cr and Au targets were placed in the magnetic field sputtering system (See Figure 19) located in the infrastructure of the RACQUT. Firstly, 10 nm Cr was coated on the glass substrate and then 100 nm gold was coated on the Cr coated substrate. 10 nm Cr and 100 nm Au coatings were deposited, respectively, with an argon flow rate of 30 sccm, keeping the coating power of 50 W for Cr and 20 W for Au coating.

Figure 19. Photograph of the magnetic field sputtering system in the infrastructure of the RACQUT.

2.3. Optimization of the parameters

2.3.1. Polymer jet formation studies

When voltage is applied, the polymer droplet suspended at the needle tip becomes charged electrically and the induced charge is evenly distributed over the droplet surface (See Figure 20). Thus, the droplet is stretched and at some point, jet occurs in the liquid stream.

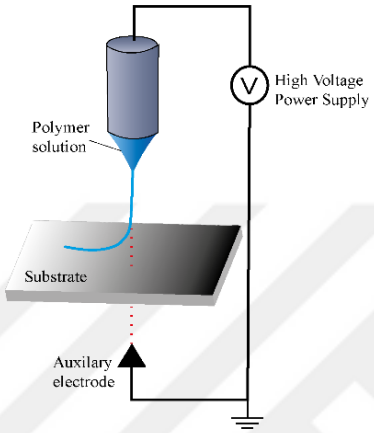

Figure 20. Schematic illustration of the general near field electrohydrodynamic process.

In addition, if the system is operated with low voltage, the polymer jet cannot start by itself. Therefore, as shown in Figure 21, polymer jet formation is initiated with the help of a tungsten micro-probe.

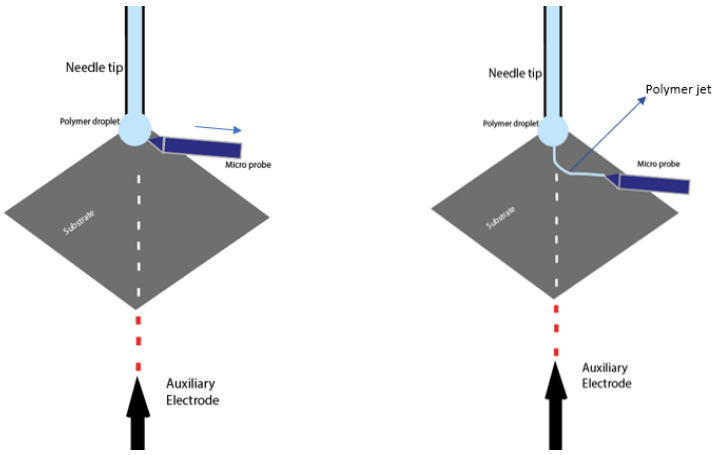

Figure 21. Diagram showing the first formation of the polymer jet as a result of the microprobe approaching the droplet for polymer jet formation.

2.3.2. Viscosity Measurements of Solutions

Viscosity studies for 2% PEO solution (MW= 4,000,000) were conducted with the JP-Selecta ST-2020R Viscometer located in Izmir University of Economics. This device measures the resistance of the material against the rotation of the disc at a known speed using a disc immersed in the analyzed material. These results are a measurement of viscosity relative to the flow characteristics of the reference point. However, since the zero-shear viscosity value given for PEO solutions in the literature could not be measured with this device, the measurements were repeated using the Hybrid Rheometer Discovery HR-2 Rheometer device located at Katip Çelebi Materials Research Center. PEO solutions prepared in the 1-5% range were placed between the parallel plate apparatus, and zero shear viscosity values were obtained by leaving a gap between the plates.

2.3.3. Process Parameters Used in Patterning

The parameters studied to reach the optimum values are as follows:

a. Applied voltage
b. Distance between needle tip collecting substrate
c. The speed of the collector
d. Molecular weight, viscosity, and type of polymer
e. Syringe Pump Feed Rate
f. Guide Electrode
g. Needle Diameter

2.3.3.1.Applied Voltage

The applied voltage plays an important role in the electrohydrodynamic process. An electric field is applied between the needle tip and the substrate in which the fiber is collected. The electric field provides necessary charge to the solution. First, the applied voltage was reduced to 1 kV and below and other variables were kept constant. A power supply with a power capacity of 10 kW was used for this purpose. The voltage was then increased up to 5 kV to investigate the effect of the voltage difference on other parameters. However, it generally kept between 0.4 kV and 1 kV.

2.3.3.2.Distance Parameters Between Needle Tip Collector Substrate

In the electrohydrodynamic system, the distances between the needle tip and the collecting substrate were studied starting from 5 mm. As a result of studies, the distance between the substrate and the needle tip was studied in the range of 0.8 mm-2 mm due to the effect on polymer jet formation, fiber diameter, and patterning.

2.3.3.3.The speed of the collector

In order to position the polymer on the substrate according to the x-y axes, the effect of the speed of the platform, which is controlled by software, on the patterning is very important. It has been observed that the patterning can be produced linearly or wavy with the platform speed. The diameters and morphologies of the fibers can be controlled with the movement speed of the platform. To determine the optimum value of the platform speed, it was studied at speeds in the range of 95 mm/min - 700 mm/min. The optimum value of the platform speed also varied according to the substrate and other parameters.

2.3.3.4.Molecular Weight, Viscosity, and Type of Polymer

Electrohydrodynamic method has been performed using various polymer solutions with different chemical and physical properties. In order to prevent arcing from the needle kept at a close distance; alignment can be made with the polymer showing super-elastic properties by applying a low electric field and using high molecular weight polymer ink solutions (Bisht et al. 2011). Due to the entangled polymer chains in the solution, the continuity of the nozzle is increased while the polymer is bent longitudinally, facilitating the continuous conversion of the polymer jet into nanofibers. Therefore, PEO-containing solutions were used in this thesis. Polyethylene oxide (PEO) (MW= 4,000,000 $g \cdot mol^{-1}$) solution was prepared at different concentrations (in the range of 1-5 wt%) to determine the optimum polymer concentration. According to the electrohydrodynamic method studies carried out with different concentrations, it was determined that the appropriate concentration value was 2 wt% in the electrohydrodynamic method as shown in the “Results and

Discussion" section. Generally, 25 ml solutions were prepared in volumetric flasks at room temperature. For the preparation of 2 wt% PEO solution, 0.5 g of PEO + 24.5 ml of ultrapure water was mixed and homogenized in a mixer for 96 hours and rested for 24 hours. In addition, electrohydrodynamic method with PEO solutions with different molecular weights is necessary to investigate the effect of molecular weight on fiber morphology and patterning of the fibers. In this regard, the patterning was carried out by preparing 4% wt. PEO solution with a molecular weight of 900,000 $g \cdot mol^{-1}$ (24 hours of rest and 96 hours of mixing).

Fiber patterning by electrohydrodynamic method was also performed using Polyvinylpyrrolidone (PVP) polymer. In this regard, an 8% wt. solution was prepared with methanol using a PVP polymer with a molecular weight of 1.300.000 $g \cdot mol^{-1}$. However, in the study, a continuous fiber formation could not be observed with a close distance (1 mm). Fiber could be produced with PVP only when long-distance and high voltage were applied.

2.3.3.5.Syringe Pump Feed Rate

The solution flow rate is another process parameter and the optimum value of the rate is the value at which the Taylor cone is stable. If the flow rate is higher than this value, bead formation and an increase in the fiber diameter were observed. The rapid solution flow causes an increase in the feed at the needle tip per unit time, as well as the fiber diameter. It has been studied with different syringe types at feed rates of 0.73 µl/h -2.5 µl/h.

2.3.3.6.Guide Electrode

The type of guide electrode is also important during the process, and either the collector must be conductive or a guide electrode must be used to generate the electric field. In the preliminary studies, a needle tip was placed under the collector to increase

the alignment of the fibers and served as a guide electrode (See Figure 22a). In addition, a conductive plate was also used (See Figure 22 b).

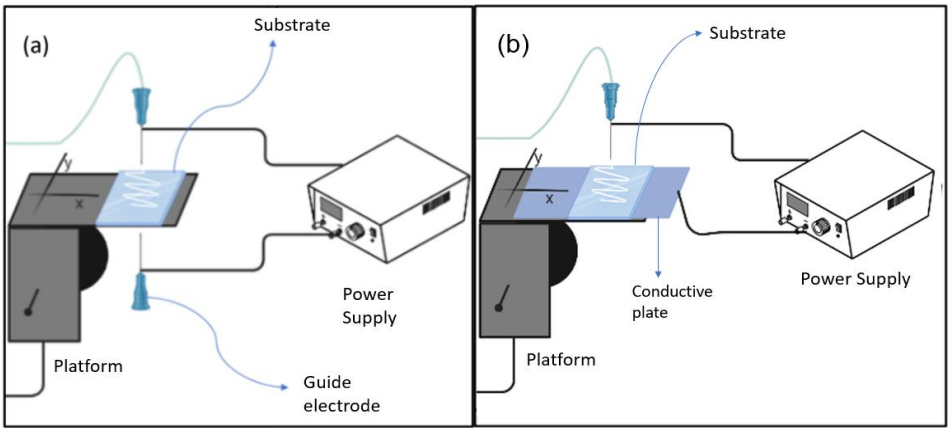

Figure 22. Schematic representation of different types of guide electrodes (a) needle tip guide electrode (b) conductive plate guide electrodes integrated into the system.

2.3.3.7.Needle Diameter

Needle diameter also affects fiber structure. It can be studied to reduce the bead formation that occurs during the fabrication of the fibers. 30 gauge needles were used by connecting with the hose of the butterfly needle. The connection was performed by the hot plastic injection method under vacuum (See Figure 23).

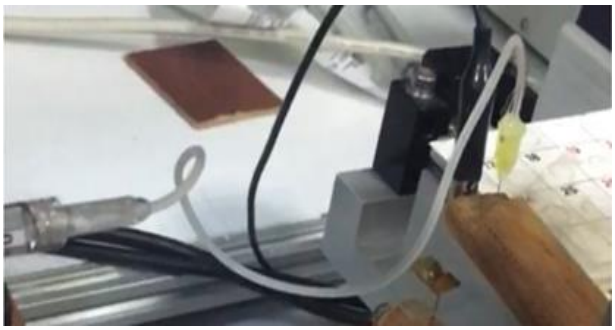

Figure 23. 30 Gauge needle and its connection with a hose.

2.3.4. Environment Parameters

During electrohydrodynamic method, ambient conditions such as temperature and humidity must be kept at constant and optimum values. Since there is no cabin with an air conditioner in which the electrohydrodynamic system is placed, the experiments were carried out in a standard laboratory environment. Under these conditions, problems were experienced in alignment of the fibers and fiber formation.

In addition, experiments were conducted to examine the effects of temperature on the adhesion of the fiber to the substrate. Using 2% PEO polymer solution, patterning studies were carried out on Cr/Au-coated glass substrates at varying temperatures. The substrates, which were heated in a controlled manner with a thermocouple, were placed in the system. While the system was operating, temperature measurements were carried out with a thermocouple. The patterning was studied when the substrate had a temperature of 80°C.

2.4. Argon Ion Beam Etching Process

After the electrohydrodynamic method patterning, the metal was stripped from the substrate by etching the metal in the uncoated areas with Ar ion etching. In order to etch the patterns obtained at this stage with the ion etching system, experiments were carried out at different time intervals to determine the appropriate etching time. The etching of the samples was performed by argon ion beam etching system, which is a custom-made set-up consisting of a turbomolecular pump (Agilent Varian Turbo-V 301), a rough pump, a multi-gas controller (MKS Instruments Type 647C), an etching chamber, an end-Hall type ion source (Advanced Energy MCIS-12), a DC power supply (Advanced Energy Pinnacle Plus), a thermocouple vacuum gauge, a closed cycle cooling system, and a cold cathode gauge controller. The operating conditions of the device were 49 W as DC power, 0.07 A as current value, and 750 V as a voltage value. The sample holder was placed at an angle of 22.5 degrees and rotated during etching with 3.2 V DC.

2.5. Removal of Polymer Process

After the ion etching process, the polymer on the pattern must be removed. Therefore, it was decided to try to remove the polymer with organic solvents (methanol, ethanol, etc.) that are known to dissolve PEO. A 2:1 methanol-water solution was prepared and heated in a controlled manner on the hot plate until it reached 50ºC. The sample was also heated on the hot plate in a glass petri dish for 2 minutes. Therefore, the polymer on the pattern was softened by increasing the temperature of the substrate. The methanol solution, which reached 50 ºC, was poured directly onto the pattern using a pipette. The sample was kept in solution for a while.

The sample taken from the solution was dried with nitrogen gas. Measurements were performed with AFM to determine whether the polymer was removed from the surface. The removal of polymer process was carried out for 14 minutes for patterning on 100 nm Ag coated SiO_2 substrate and 40 minutes for patterning on 10 nm Cr + 100 nm Au coated glass substrate

2.6. Electrical Characterization Method

The resistance is a measurement of the material's ability to prevent the flow of electrical current (Ohm's Law: V = IR). In order to determine the resistance of the materials, a DC current was passed through a material with resistance (R). The intensity of the electrical current (I) in the material due to this electric field, and the decrease of the potential drop (V) between two selected points are needed. The resistance (R) was found by the ratio of the current (I) flowing through the material and the voltage (V) formed.

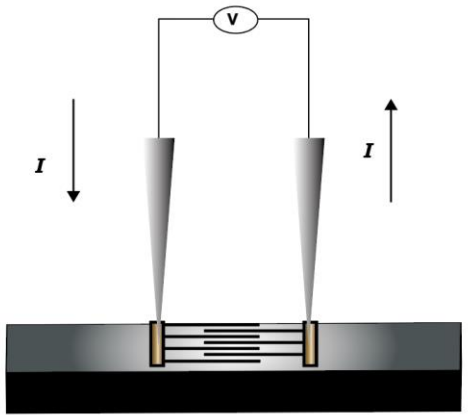

Figure 24. Schematic illustration of two-point probe method.

Two-point probe electrical conductivity measurement was performed with two metal-conductive contact probes (See Figure 24). To determine the resistance, the value of I and V must be determined directly. The R-value obtained in the resistance determination measurement made with this method may also include the resistance of the contacts (Loh, 2008).

Electrical measurements were conducted by contacting the probes to both sides of the electrodes obtained in an interdigitated arrangement. In order to allow the probes to contact both sides of the interdigitated pattern, gold was deposited on the edges of the sample with the thermal evaporation method using a shadow mask (See Figure 25). IV measurement was made by connecting the probes to these metal strips. The current change was measured by applying a voltage at certain intervals and an I-V curve was obtained.

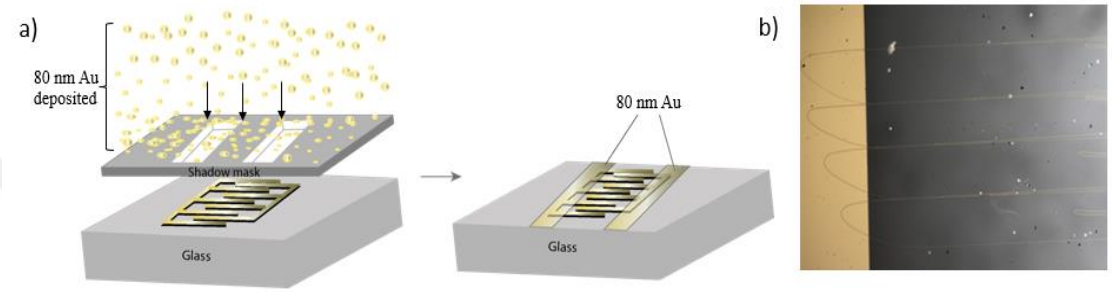

Figure 25. (a) Schematic illustration and (b) optical microscope image of sample that Au was deposited on both edges by Thermal Evaporation method.

2.7. Characterization

In order to examine the structural properties of the nanofibers obtained as a result of patterning, Quanta 250 FEG within IZTECH Materials Research Center and Carl Zeiss 300VP model scanning electron microscope (SEM) within Katip Çelebi Materials Research Center were used. Image analyzes were performed with the Olympus SZ61 and Nikon Eclipse LV150 optical microscopes within Research and Application Center for Quantum Technologies (RACQUT). For the elemental distribution of nanofibers, Oxford Aztec brand Energy Dispersive X-ray (EDX) detector mounted on SEM was used. Also for line edge roughness measurement,were analyzed by Lacerm which is a Matlab-based image processing software. Two Point Probe Method (Hoiki IM3590) was used for electrical measurement. In order to determine the thickness and sample surfaces of the fibers, Hitachi brand AFM5100N model Multi 75Al-G AFM type within İzmir University of Economics was used (See Figure 26).

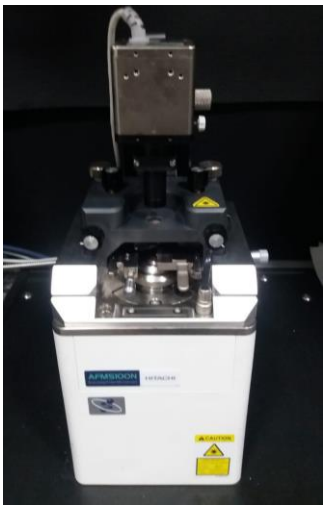

Figure 26. HITACHI Multi-Function SPM Unit AFM5100N.

CHAPTER 3: RESULTS AND DISCUSSION

3.1. Studies to Determine Optimum Solution Viscosity for the System

Zero shear viscosity values were obtained for PEO solutions prepared in the range of 1-5% by weight (See Table 2). According to the literature, these values were given as 1.33 Pa•s for 1% PEO solution, 28.7 Pa•s for 2% PEO solution, and 111 Pa•s for 3% PEO solution (Bisht et al. 2011). The zero shear viscosity for the 2% PEO solution, deviated by 0.77% compared to the literature. In other solutions, this difference deviated by 5.83% for 1% PEO solution and 15.92% for 3% PEO solution. These deviations were thought to be due to methodological differences in preparing the solutions.

Table 2. Zero shear viscosity values of PEO solutions (MW= 4,000,000) with different concentrations

Polymer concentration	Zero shear viscosity (Pa•s)
%1 PEO	1.4076
%2 PEO	28.4877
%3 PEO	128.671
%4 PEO	351.759
%5 PEO	424.025

Before starting the viscosity studies depending on the substrate temperature, the effect of the viscosity of the 2% PEO solution on the temperature was investigated with a rheometer. In this regard, viscosity change was observed by increasing the temperature of the solution from room temperature to 80ºC (determined as the maximum temperature due to the water content of the solution) by 5ºC per minute. The change in the viscosity of the solution was determined to be 0.133 when it reached 80ºC (See Figure 27). The patterning was started when the substrate was at 80ºC by

integrating thermocouples into the system, and changes in the patterning and fiber structure were detected as decreasing of the temperature of the substrate.

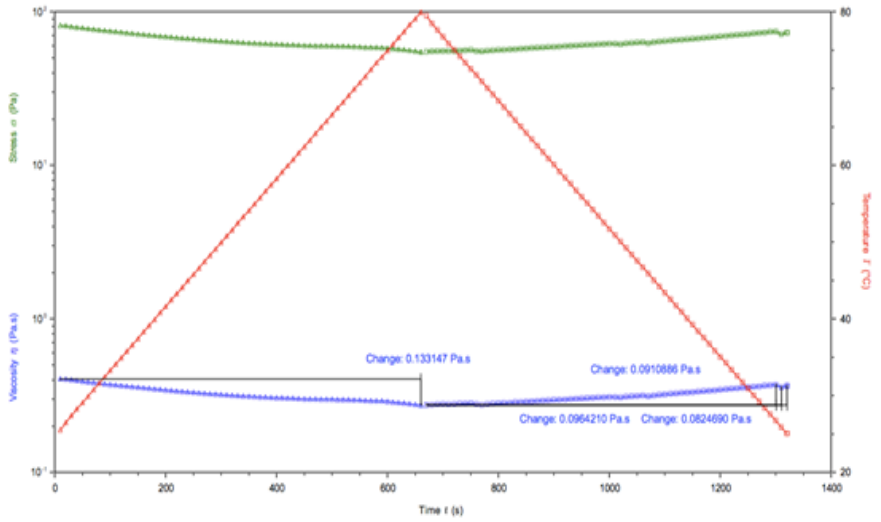

Figure 27.Effect of viscosity and stress of 2% PEO solution on temperature.

3.2. Patterning Studies with Needle Tip Guide Electrode

The optimization studies were carried out in the electrohydrodynamic method with the auxiliary electrode method. A needle tip was added as a guide electrode 1 mm below the substrate and aligned with the upper needle. It was studied on Si/SiO_2 substrate with 1 kV voltage difference and 2.5 µL/h syringe pump flow rate, collector speed of 95 and 250 mm/min.

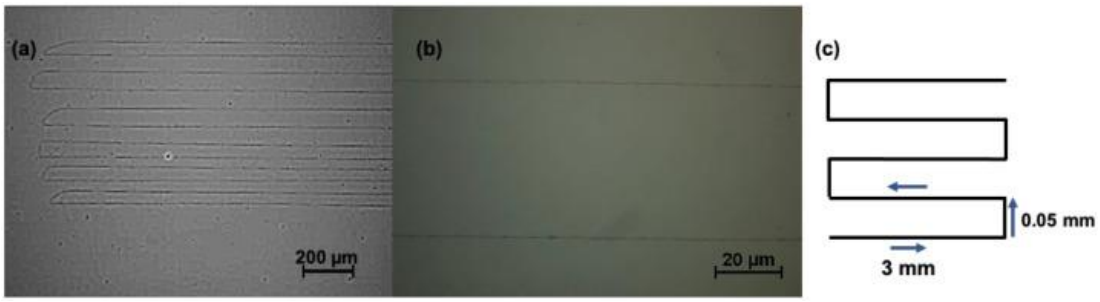

Figure 28. Optical microscope images of the fibers patterned with 95 mm/min platform speed(a) 20X magnification (b) 100X magnification and (c) the image of the desired design (Source: Noori et al., 2021).

At the smallest width, about 0.35 μm, the fibers formed a spiral structure due to the low collector velocity. Although the fibers in Figure 28b progressed in a more linear and stable structure, the sharp corner structures were not as in the desired pattern. Therefore, the patterning was performed at a higher platform speed. In the patterning at 250 mm/min platform speed, the spiral structure was not formed due to the high platform speed. However, a pattern like the design shown in Figure 28c could not be obtained. As a simpler shape, the grid pattern was printed (See Figure 29).

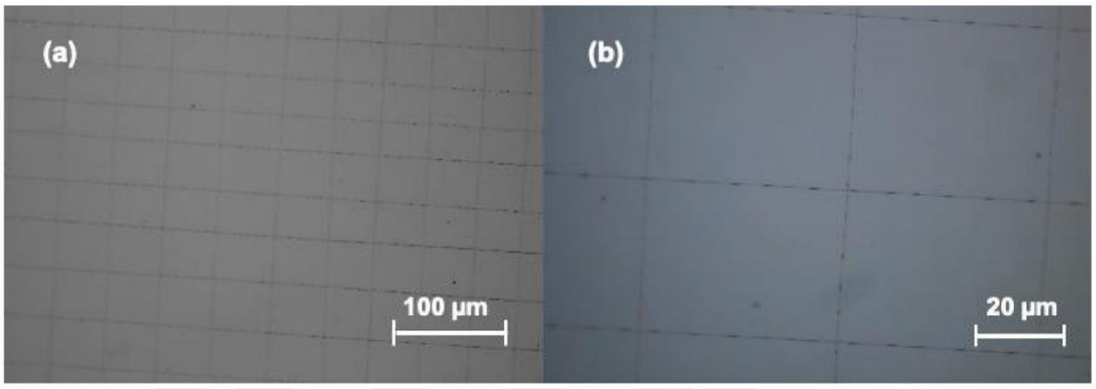

Figure 29. Optical microscope images of the fibers patterned with 250 mm/min platform speed (a) 20X magnification (b) 100X magnification (Source: Noori et al., 2021).

In the auxiliary electrode method, the desired precision patterning could not be achieved with applied voltage due to the second needle being mounted under the substrate. Therefore, patterning was performed with a grounded substrate method. This method allowed patterning by forming thinner fibers at lower voltage values.

3.3. Patterning Studies on 100 nm Ag Coated SiO_2 Substrates

Optimization studies were carried out to determine the appropriate parameter values for patterning. To print precisely at lower voltage, the patterning was applied with the grounded substrate method. Once the patterns were obtained, the next step was removing the metal from the substrate by etching the metal by Argon ion etching. Therefore, patterning was studied on SiO_2 substrates coated with 100 nm Ag.

The voltage difference was studied in the range of 0.4-0.6 kV to have flat and fine fibers on silver-coated SiO_2 substrates by electrohydrodynamic technique. The optimum speed at this voltage difference was determined as 700 mm/min platform

speed. Three examples were prepared to investigate the effect of voltage differences on fiber formation (See Table 3). The distance between the sample and the needle tip was kept as 1 mm (Noori et al., 2021).

Table 3. Samples prepared with 2% by weight PEO solution at different voltage values

Sample	Applied Voltage	Platform Speed
Sample 1	0.4 kV	700 mm/min
Sample 2	0.5 kV	700 mm/min
Sample 3	0.6 kV	700 mm/min

SEM images of three different samples (See Figure 30) show that increasing the applied voltage leads to an increase in fiber diameter and also increases the number of bead-like structures present in the fiber structure. As shown in Figure 30, the fibers with the desired size and the smallest dimension were produced by applying 0.4 kV. First, all samples were etched by the ion etching technique for 5 minutes. The samples were then etched for an additional two minutes to remove any remaining silver, as the EDX results (See Figure 31a) showed that silver residue remained in the non-fiber coated sections. EDX results (See Figure 31b) after 7 min etching showed no silver dispersion in the non-fiber area of the sample.

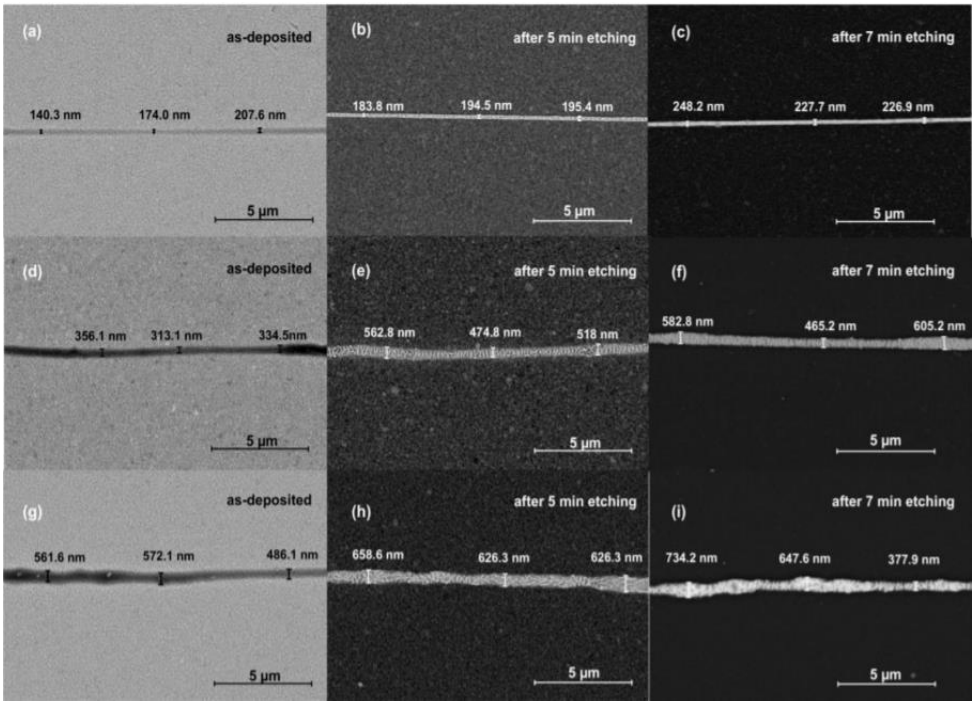

Figure 30. SEM images of the printed patterns: (a–c) Sample 1 at 0.4 kV, (d–f) Sample 2 at 0.5 kV, and (g–i) Sample 3 at 0.6 kV (Source: Noori et al., 2021).

As seen in Figure 25, thinner fibers with a diameter in the range of 208.7 ± 30.3 nm were achieved at the voltage 0.4 kV. Increasing the voltage resulted in a doubling of the fiber sizes. This confirms that fiber diameters could be controlled by the applied voltage. After etching, the variation in fiber thickness remained almost constant. The reason for the increase in fiber thickness after 5 minutes of argon ion etching is due to deviations since the average width analysis regions are different after each process.

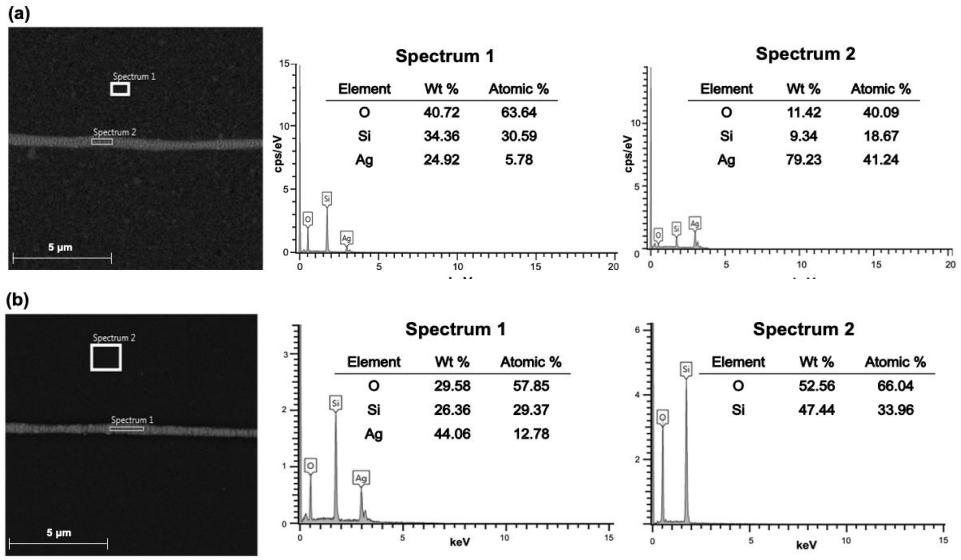

Figure 31. EDX results of sample 2 (at 0.5 kV): (a) After 5 min etching (b) After 7 min etching (Source: Noori et al., 2021).

As shown in the EDX results, silver residues were determined after 5 minutes of etching (See Figure 31a) and after 2 more minutes of etching, it was observed that there was no silver left outside the fiber-coated area (See Figure 31b).

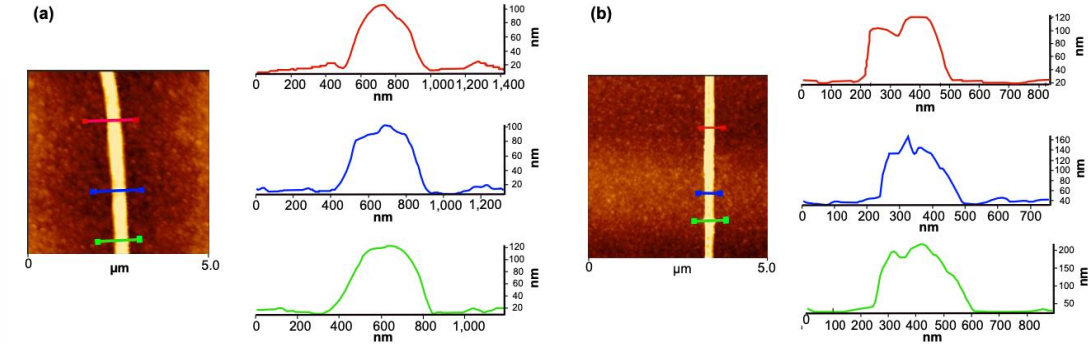

Figure 32. AFM image and height profile of Sample 1 obtained with 400 V voltage, 700 mm/min platform speed, and 1 µl/hr syringe pump feed rate: (a) fiber before etching (b) fiber after 7 min etching (Source: Noori et al., 2021).

The morphology and size of the fibers were determined by AFM before and after the etching process (See Figure 32). Fiber thickness and diameter before argon ion etching were 93.47 ± 26.96 nm and 715.63 ± 299.6 nm, respectively (calculated from 72 data points). On the other hand, after 7 minutes of argon ion etching, the nanofibers had a thickness of 117.36 ± 33.43 nm and a diameter of 518.98 ± 193.79 nm (calculated from 108 data points). In the etching process, fibers were slightly etched while protecting the metal, and even the silver was slightly etched in the y-direction. This result confirms that the longer the argon-ion etching process time can further reduce the sizes of the silver layer and even break the nanofibers. In addition, mean value of Line Edge Roughness of sample at 0.4 kV after 7 minutes etching was measured as 22.58 ± 3.57 nm from 15 different spots.

3.4. Patterning Studies on 10 nm Cr +100 nm Au Coated Glass Substrates

3.4.1. Patterning Using 3%, 4%, 5% Density PEO Solutions by Weight

It is important to determine the optimum solution concentration for fiber thicknesses and patterning. On glass substrates with 10 nm Cr + 100 nm Au coating, electrohydrodynamic method studies were carried out using PEO solutions at 3%, 4%, and 5% by weight densities, with the parameters given in Table 4.

Table 4. The values studied for the distance between the needle tip and the collector, the applied voltage, the feeding speed of the syringe pump, and the speed of the platform with 3% by weight PEO solution

Sample	Distance (mm)	ΔV (kV)	PR (μL/h)	Substrate	Platform speed (mm/min)
S4	1	1	0.73	10 nm Cr +100 nm Au coated glass	90
S5	0.8	0.9	0.73	10 nm Cr +100 nm Au coated glass	90
S6	0.8	1	0.73	10 nm Cr +100 nm Au coated glass	90

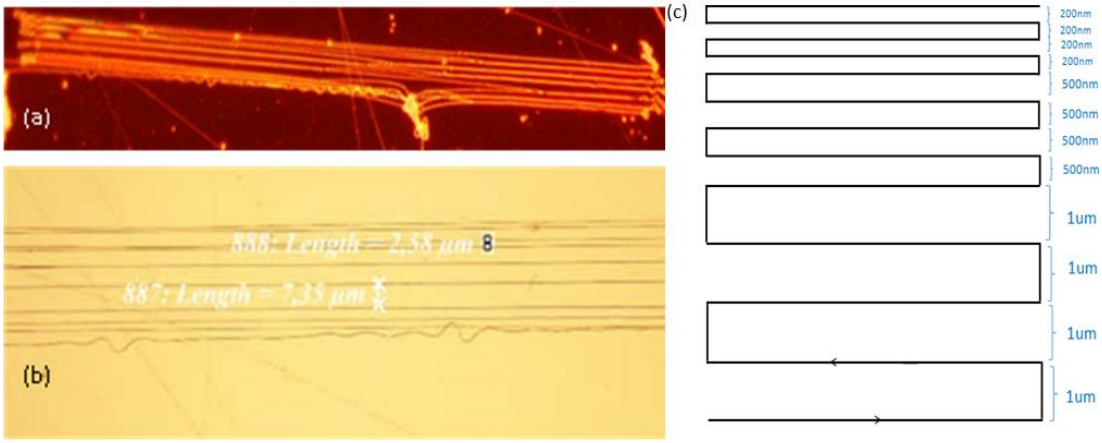

Figure 33. (a), (b) Images of the S4 sample produced according to the parameters shown in Table 4 from two different optical microscopes and the shape and (c) direction of the pattern to be produced.

In the optical microscope image in Figure 33a, except for the pattern, the reflected lines and dots originated from the surface. In addition, distortions were observed in the lower part of the pattern due to a particle remaining on the surface.

When the 3% wt PEO solution was used, thicker fiber was formed than the fibers obtained from 2% wt PEO solution. In low voltage values, fluctuations in fiber structure due to viscosity (See Figure 34b) were observed. However, 3% by weight PEO solution could be preferred for micro-scale fiber production due to the success of the fibers in linear structure and pattern formation (See Figures 33a and 34a).

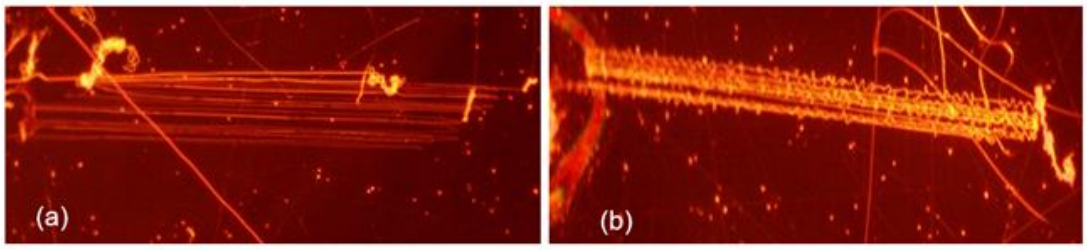

Figure 34. Optical microscope images of (a) S5 and (b) S6 produced according to the parameters shown in Table 4.

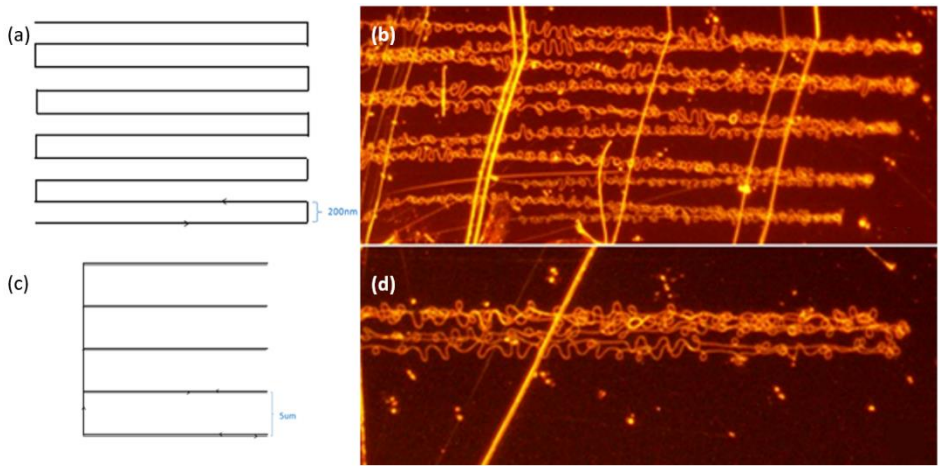

Figure 35. Directions and dimensions of the patterns planned to be produced for samples (a)S7, and (c) S8; optical microscope images of (b) S7, and (d) S8 samples produced according to the parameters shown in Table 5.

Table 5. Parameters studied for 4% by weight PEO solution, the distance between the needle tip and collector, applied voltage, feeding speed of syringe pump, and speed of the platform

Sample	Distance (mm)	ΔV (kV)	PR (μL/h)	Substrate	Platform speed (mm/min)
S7	1	1	0.73	10 nm Cr +100 nm Au coated glass	90
S8	1	0.9	0.9	10 nm Cr +100 nm Au coated glass	90

Except for the pattern shown in Figure 35b, and 35d, the dots and lines were due to pinholes formed during coating and scratches during the cleaning of the substrate. Optical microscope images of the patterns produced according to the values given in Table 5 are given in Figure 35. The formation of wavy fibers was observed due to the high viscosity (~351.8 Pa•s) of the 4% wt. PEO polymer solution. It has been concluded that the fibers had a fluctuating movement due to the increase in viscosity and the difficulty of exiting the needle tip. Likewise, fiber rupture occurred during patterning due to high viscosity, external air flows, and freezing of the polymer. The pattern shown in Figure 35c could not be fully formed (See Figure 35d). However, since the viscosity value of 5% wt. PEO polymer solution was ~424 Pa•s, the polymer has been forced out of the syringe and leaks occurred in the needle hose connections. Therefore, it was decided that patterning cannot be done with a 5% PEO solution.

3.4.2. Studies Using 2% by Weight PEO Polymer Solution

3.4.2.1. Patterning by electrohydrodynamic method at Different Temperatures

Patterning studies were carried out at varying temperatures on glass substrates coated with 10 nm Cr + 100 nm Au using 2% by weight PEO polymer solution. Heated substrates were placed in the system and temperature measurements were made with a thermocouple. The patterning was done when the temperature of the substrate reached 80°C.

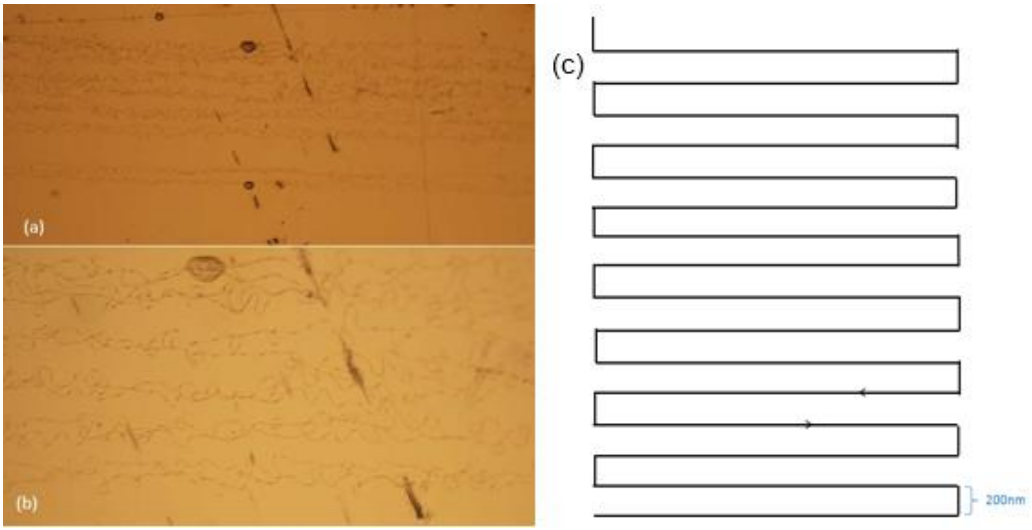

Figure 36. Images of the S9 sample produced according to the parameters shown in Table 6 with an optical microscope (a) at 20x magnification and (b) at 50x magnification, and (c) the shape and direction of the pattern to be produced.

Table 6. Parameters studied for 2% by weight PEO solution, the distance between the needle tip and collector, applied voltage, feeding speed of syringe pump, and speed of the platform

Sample	Distance (mm)	ΔV (kV)	PR (μL/h)	Substrate	Platform speed (mm/min)	Temperature (°C)
S9	1	0.9	0.95	10 nm Cr +100 nm Au coated glass	90	80

Optical microscope images of the sample produced according to the values given in Table 6 are shown in Figure 36. The substrate temperature changed the

viscosity of the polymer solution and evaporated the water in the solution. As a result, fibers showing dispersion on the surface were obtained. In addition, bead formations were observed in the fibers.

3.4.2.2. Optimization Studies Using 2% PEO solution by weight

In the studies with Ag coated glass substrates, the desired results were obtained in the fiber alignment studies when the voltage difference was below 1 kV and the distance between the needle tip and the collector was kept 1 mm. Therefore, it has been continued to work with these values in glass substrates coated with 10 nm Cr + 100 nm Au. However, the platform speed was changed because patterning was studied in an interdigitated structure instead of straight fibers. It was determined as 90 -160 mm/min (changes with the size of the pattern), which was slower than the values used in flat fiber production to allow the formation of the pattern. When a high pump feed rate is used, it is necessary to operate at low voltage values. When high voltage is applied with a high pump feed rate, polymer droplets accumulating at the needle tip can adhere to the substrate surface due to close distance.

Table 7. Parameters studied for 2% by weight PEO solution, the distance between the needle tip and collector, applied voltage, feeding speed of syringe pump, and speed of the platform

Sample	Distance (mm)	ΔV (kV)	PR (μL/h)	Substrate	Platform speed (mm/min)
S10	1	0.7	0.73	10 nm Cr +100 nm Au coated glass	90
S11	1	0.6	0.83	10 nm Cr +100 nm Au coated glass	90

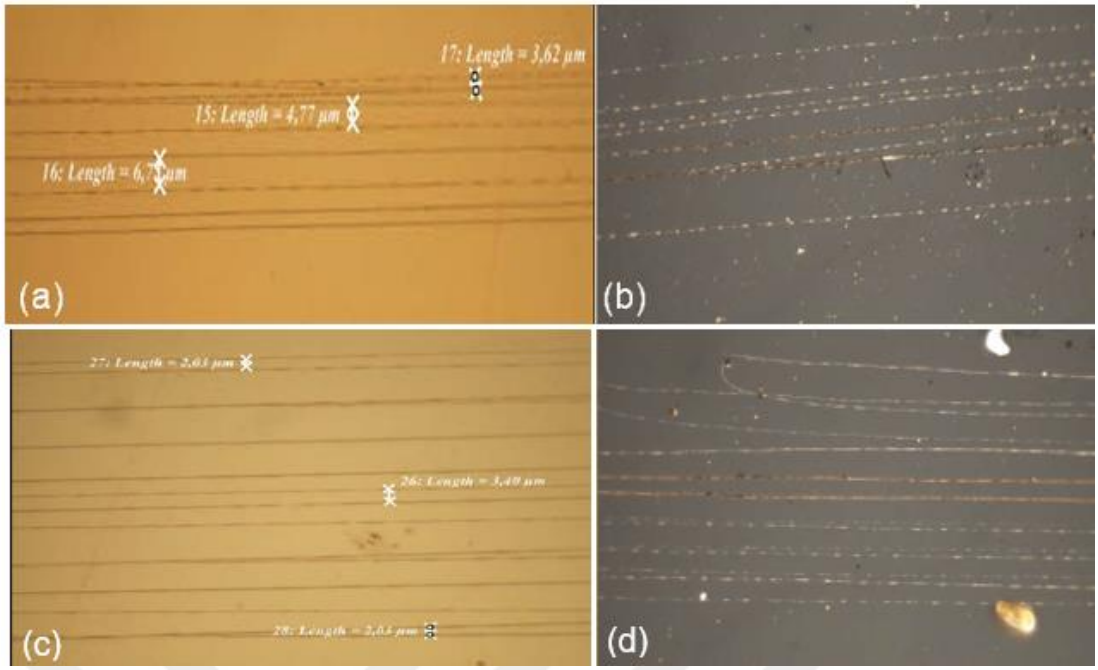

Figure 37. S10 and S11 samples were produced according to the parameters shown in Table 7: (a), (c) before, and (b), (d) after argon ion etching.

It was planned to position the fibers in parallel at 200 nm intervals (See Figure 37a, 37b). It was observed that the distances between the fibers could not be adjusted. In addition, large gaps between the fibers and breakage of the fibers occurred during patterning. Therefore, it was concluded that the distances between the fibers could not be reduced to 200 nm in studies on glass substrates coated with 10 nm Cr + 100 nm Au.

In addition, after electrohydrodynamic method patterning, the removal of the metal from the substrate was studied by etching the Au metal in the non-fiber-coated areas with Ar ion etching (See Figure 37b and 37d). Ar ion etching was carried out for 15 minutes. However, it was understood from the dashed line formations in the fibers that some Au metal was also removed along with the polymer on the pattern. Based on these results, it was decided to decrease the duration of the Ar ion beam etching process.

3.4.2.3. Patterning Studies in Interdigitated Order

Interdigitated electrodes used in impedance or conductivity measurements were produced in micrometer sizes with different techniques. The developed electrospinning was aimed to produce interdigitated electrodes on a nanometer scale. For this pattern structure, the fiber should be cut in the middle electrode area of the pattern and draw a line like a comb. However, when the fiber was connected to the surface, even if the fiber was broken by cutting the voltage, manual assistance is required to reconnect the fiber. Although the fiber could be obtained without manual assistance at very high voltage values, in this case, more than one fiber was formed or the fibers were thicker than expected. In addition, the drop accumulated at the tip of the needle due to the high tension dropped on the substrate and destroyed the Taylor cone. Another problem was the viscosity changed due to climatization problems in ambient conditions. In this case, sometimes the fiber did not break even if the voltage was cut. Therefore, production was started in the form of the fiber returning once again the route it completed after moving in a line (See Figure 38a). Studies were carried out with the design with 200 nm intervals between the fibers. However, there were situations where the fibers could not rotate on the same line while returning, so they formed irregular structures by intertwining. This makes it impossible to produce interdigitated structures on the nanometer scale intervals. Therefore, the patterns prepared with electrode spacings of 2 µm, 5 µm, 10 µm, 100 µm, and 200 µm were studied to create the interdigitated electrodes.

Table 8. Parameters studied for 2% by weight PEO solution, the distance between the needle tip and collector, applied voltage, feeding speed of syringe pump, and speed of the platform

Sample	Distance (mm)	ΔV (kV)	PR (µL/h)	Substrate	Platform speed (mm/min)
S12	1	0.7	0.85	10 nm Cr +100 nm Au coated glass	260
S13	1.2	1	0.85	10 nm Cr +100 nm Au coated glass	90

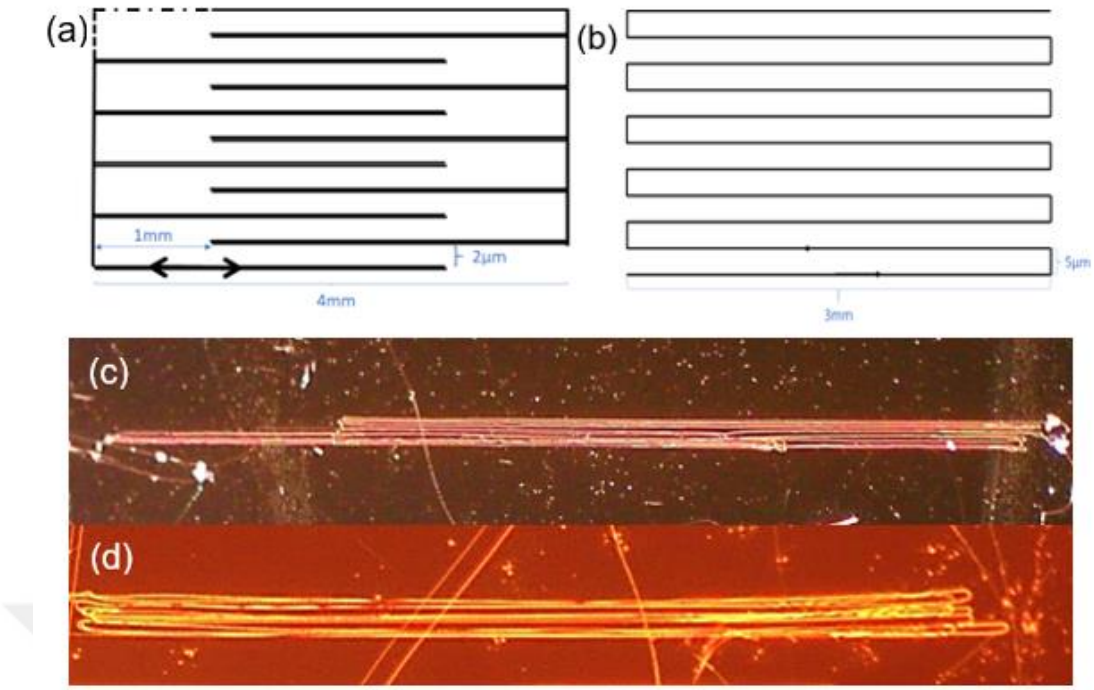

Figure 38. Shape and directions of the pattern planned to be produced and optical microscope images of the pattern structures produced, respectively: (a), (c) S12 sample, and (b), (d) S13 sample

As shown in Figure 38c, and 38d, the patterns with 2 and 5 µm electrode intervals were studied. Despite the linear progression of the fibers, it was observed that they went out of the desired pattern and passed over each other. The desired pattern could not be created in these intervals.

The patterns with an interval of 10 µm were also worked, but the fibers still crossed with each other. Therefore, two-part patterning was studied as the right and left sides to create the interdigitated structure. It is aimed to create two comb structures as placed in an interdigitated form.

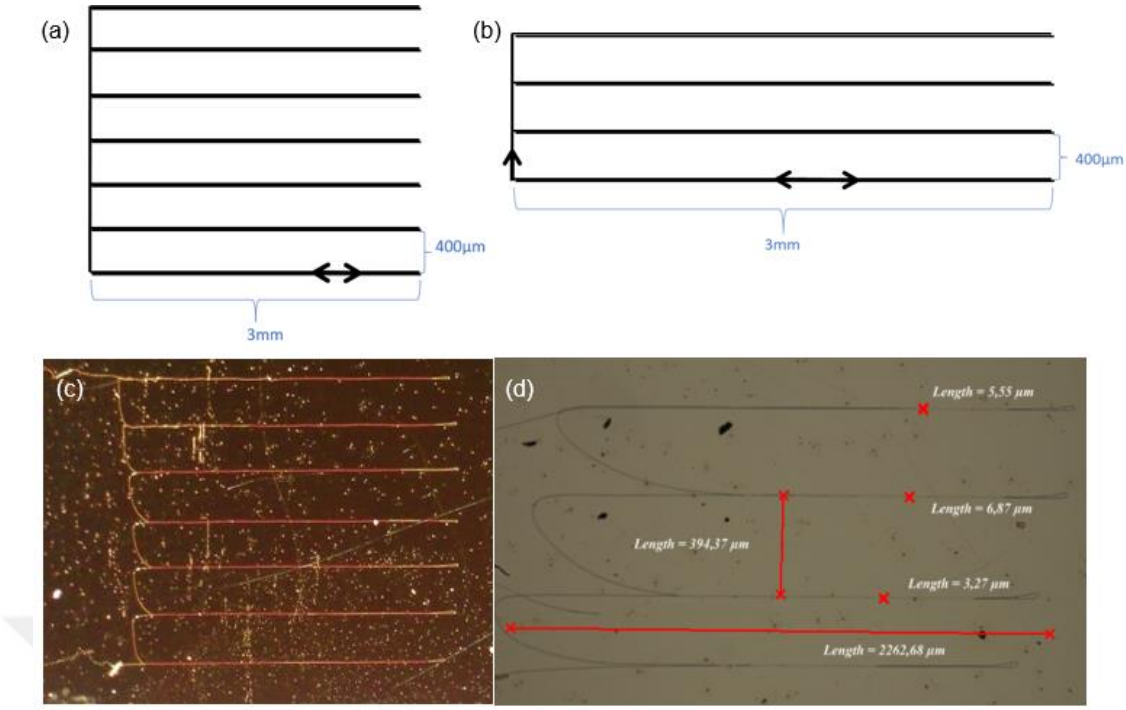

Figure 39. Shape and direction of the pattern planned to be created and optical microscope images of the pattern produced: (a), (c) S14 and (b), (d) S15.

Table 9. Parameters studied for 2% by weight PEO solution, the distance between the needle tip and collector, applied voltage, feeding speed of syringe pump, and speed of the platform

Sample	Distance (mm)	ΔV (kV)	PR (µL/h)	Substrate	Platform speed (mm/min)
S14	1	0.78	1	10 nm Cr +100 nm Au coated glass	160
S15	1	0.78	1	10 nm Cr +100 nm Au coated glass	150

The patterns with 400 µm electrode spacings aligned as planned are shown in Figure 39. Due to the image analysis of these samples with an optical microscope, it was understood that the alignment made at 400 µm intervals was suitable for production in interdigitated form. When the reverse version of this pattern was positioned opposite, the pattern was obtained in an interdigitated pattern at 200 µm intervals.

In another study, 400 µm interval patterning, which was tried in the first stage, was positioned opposite to each other to create interdigitated patterning. The pattern

shown in Figure 40a created at 200 µm intervals was produced using the parameters given in Table 10.

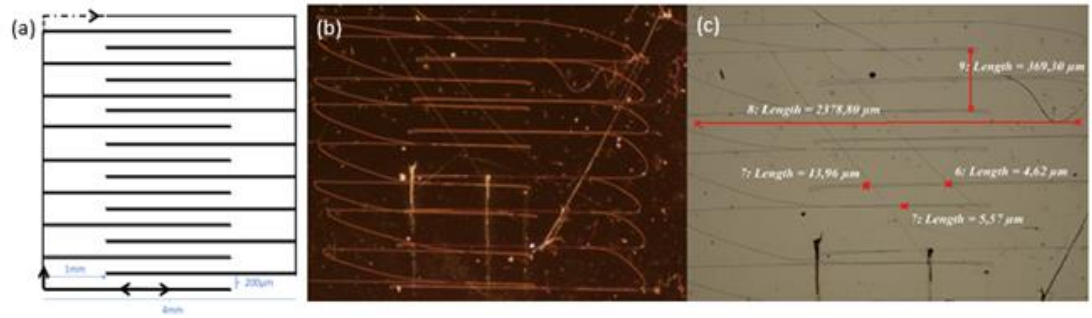

Figure 40. (a) Shape and directions of the pattern planned to be produced and (b), (c)two different optical microscope images of S16 sample produced with this pattern.

Table 10. Parameters studied for 2% by weight PEO solution, the distance between the needle tip and collector, applied voltage, feeding speed of syringe pump, and speed of the platform

Sample	Distance (mm)	ΔV (kV)	PR (µL/h)	Substrate	Platform speed (mm/min)
S16	1	0.75	1	10 nm Cr +100 nm Au coated glass	100

According to the images obtained with an optical microscope in Figures 40b and 40c, sharp turns could not be formed in the corners of the S16 sample due to variables such as air flows and platform speed. However, it was observed that the study with this patterning had the promising results and the patterning studies were continued by increasing the platform speed.

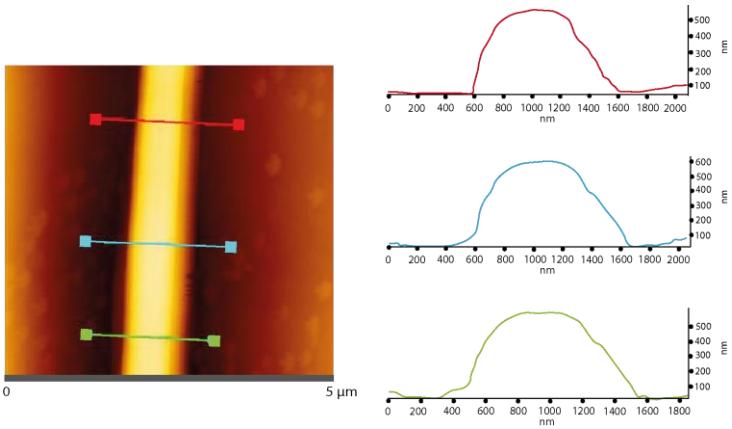

Figure 41. AFM image of the overlapped fibers of the S16 sample produced according to the parameters shown in Table 10.

In the AFM results in Figure 41, it was shown that the fiber formed by combining two fibers by returning over the same fiber. The fiber width was approximately 1 µm.

Table 11. Parameters studied for 2% by weight PEO solution, the distance between the needle tip and collector, applied voltage, feeding speed of syringe pump, and speed of the platform

Sample	Distance (mm)	ΔV (kV)	PR (µL/h)	Substrate	Platform speed (mm/min)
S17	1	0.75	0.95	10 nm Cr +100 nm Au coated glass	160
S18	1	0.78	1	10 nm Cr +100 nm Au coated glass	130

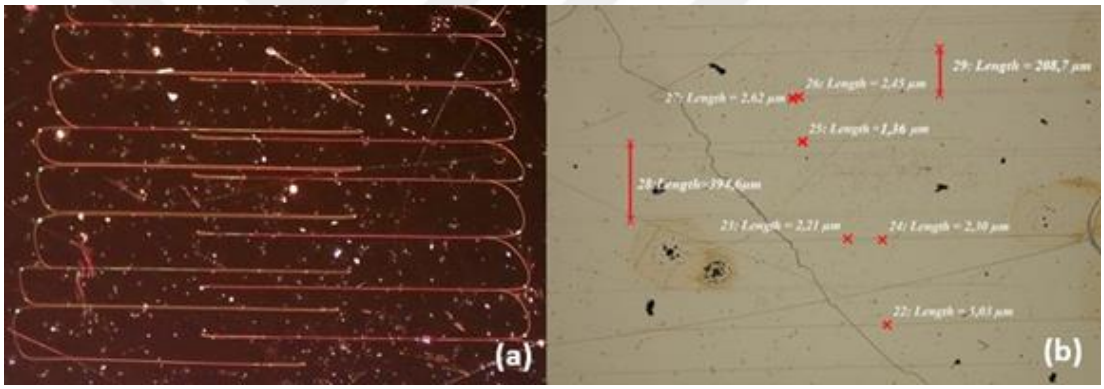

Figure 42. Optical microscope images of (a) S17 and (b) S18 samples produced according to the parameters shown in Table 11.

As shown in the two different samples given in Figure 42, the desired interdigitated pattern results were successfully achieved by increasing the platform speed compared to the previous conditions. After, the pattern is obtained, the electrodes should not contact each other. Therefore, after the designed pattern was created, the area of the pattern that needs to be removed with dots is given in Figure 40a. The separation from the upper left corner was performed by manually lifting it with a probe under an optical microscope. Other successful results obtained with the values in Table 12 were also shown in Figure 43b, 43c, and 43d. The samples S20 and S21 were obtained by aligning them according to the pattern given in Figure 43a.

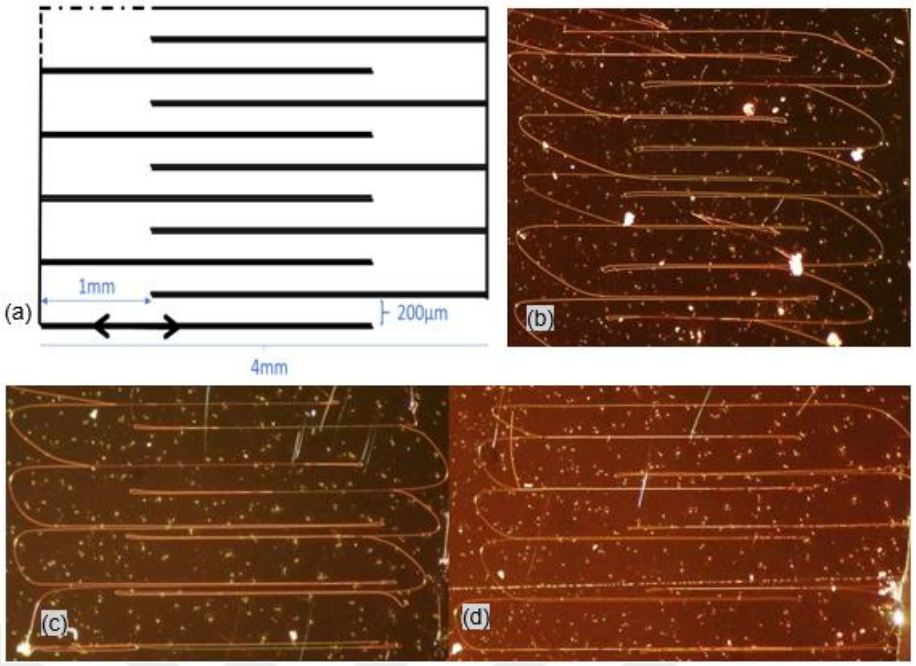

Figure 43. The shape and direction of the pattern to be produced (a) and the optical microscope images samples of (b) S19, (c) S20, and (d) S21 were produced according to the parameters given in Table 12.

Table 12. Parameters studied for 2% by weight PEO solution, the distance between the needle tip and collector, applied voltage, feeding speed of syringe pump, and speed of the platform

Sample	Distance (mm)	ΔV (kV)	PR (µL/h)	Substrate	Platform speed (mm/min)
S19	1.5	0.8	0.95	10 nm Cr +100 nm Au coated glass	120
S20	1	0.78	1	10 nm Cr +100 nm Au coated glass	140
S21	1	0.7	1	10 nm Cr +100 nm Au coated glass	160

3.5. Optimization Studies for the Ar Ion Beam Etching

After the desired patterns were obtained successfully, the next step was to remove the gold outside the area protected by the polymer. The patterns obtained at this stage were etched with the argon ion beam etching method. It was tried to

determine the optimized etching time by applying etching durations. Achieving optimized values with the ion etching system has been a very difficult process. During excessive etching times, gold was removed together with the polymer on the surface, and fractures were observed in the electrodes. If the fiber thicknesses are too thin or the fiber cannot adhere to the surface, distortions in the patterns will occur in the etching process. It was determined that the optimum value of the etching time for glass substrates coated with 100 nm Au + 10 nm Cr was 9 min at the first stage.

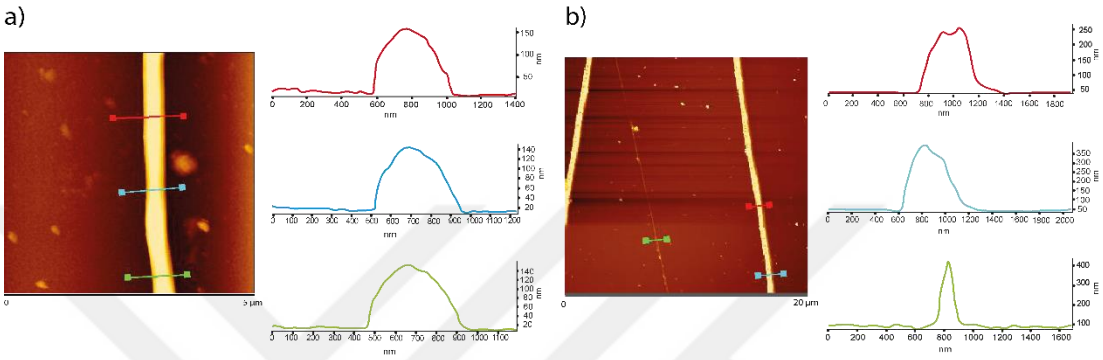

Figure 44. S18 sample AFM measurements (a) before and (b) after 9 min etching.

The S18 sample was first etched by ion etching for 5 minutes. It was observed that the metal on the surface outside the polymer-coated area could not be completely removed. Then, etching was carried out for 2 more minutes under the same conditions. However, since the gold on the surface could not be removed, etching was performed for 2 more minutes again under the same conditions. As a result of the etching process, it was determined that the optimum etching time was 9 minutes. The thickness of the fiber, which was 350 nm thick before etching, decreased to approximately 200 nm after etching (See Figure 44a and 44b). In this context, it is understood that the thickness value of 200 nm consists of 90 nm polymer in addition to the 110 nm metal coating.

As a result of gradually argon ion etching studies, 9 minutes was determined as the optimum condition for metal etching. However different results were obtained in a single step of 9 minutes etching. It is thought that these results are caused by the changes in the voltage values experienced from time to time in the etching system. In this context, it was decided to carry out the Argon ion beam etching process in the form of 5 min + 2 min + 2 min.

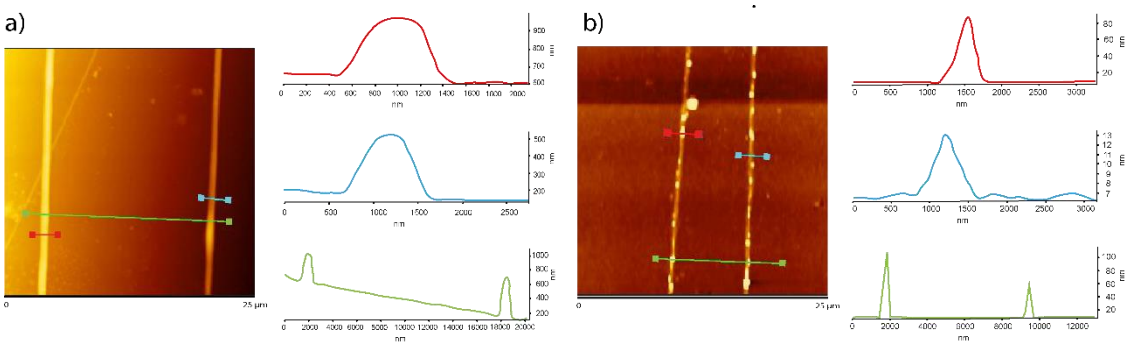

Figure 45. S16 sample AFM measurements (a) before and (b) after 9 min etching.

S16 sample was etched with argon ion for 9 minutes. According to the AFM measurements before and after etching (See Figure 45), the fibers with a thickness of approximately 300 nm became 80 nm after etching. Along with the polymer, the Au under the polymer was also removed and some ruptures were observed. In the measurements taken from the regions where there are disconnections, regions, where the electrode thickness decreased to 10 nm, were detected.

In the S20 sample, using the same parameters, etching was performed for 9 minutes at once. It was observed that the metal still remained in the non-fiber-coated areas on the sample surface. Since the fiber thickness remained in the range of 350-400 nm according to the AFM analysis, the sample was etched for 2 more minutes. Thus, for this example, the argon ion beam etching process was applied in the form of 9 min + 2 min in total.

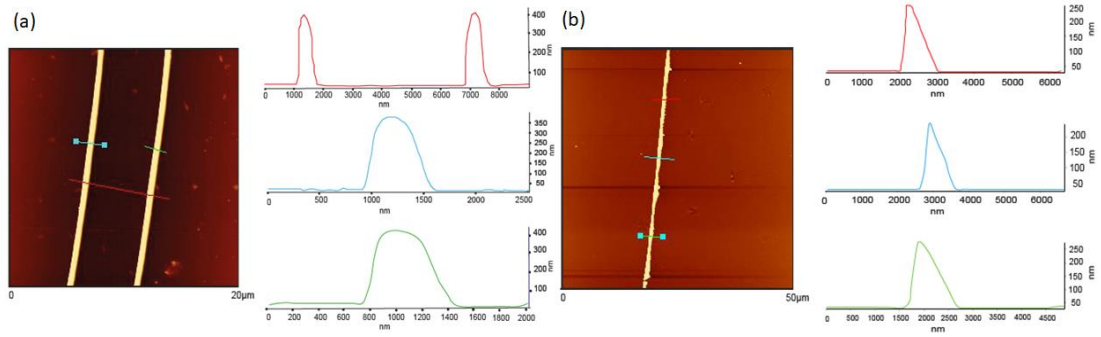

Figure 46. S20 sample AFM measurements (a) before and (b) after 11 min etching.

When the AFM measurements were examined, the fiber thickness, which was about 300 nm, decreased to 200 nm after the ion etching process (See Figure 46). It was observed that with the 9 min + 2 min etching process, approximately 100 nm of the polymer was etched, as well as the uncoated areas. As a result, it was decided to apply argon ion etching gradually in the range of 9-11 minutes depending on the thickness of the fiber.

The S22 sample was etched in three stages with Argon ion etching at 5 + 2 + 2 minutes. The optical microscope images of the S22 sample, patterned with the parameters given in Table 13, before and after Argon ion etching are shown in Figure 47.

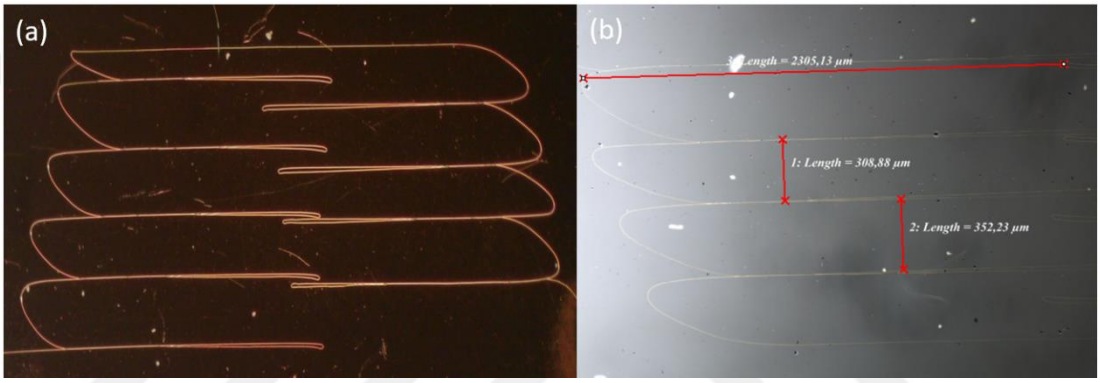

Figure 47. Optical microscope images of S22 sample (a) before and (b) after 9 min Argon Ion Etching.

Table 13. Parameters studied for 2% by weight PEO solution, the distance between the needle tip and collector, applied voltage, feeding speed of syringe pump, and speed of the platform

Sample	Distance (mm)	ΔV (kV)	PR (µL/h)	Substrate	Platform speed (mm/min)
S22	1.5	0.8	1	10 nm Cr +100 nm Au coated glass	160

In detailed optical microscope analyzes, no deformation was observed in the fibers during the etching phase. Due to polymer viscosity and environment parameters, full bonding could not be achieved in the patterning stage by returning on the same fiber. However, no rupture was observed for electrical characterization. Measurements with AFM also confirmed optical microscope observations. AFM measurements

showing the fiber morphology before and after argon ion beam etching are shown in Figure 48.

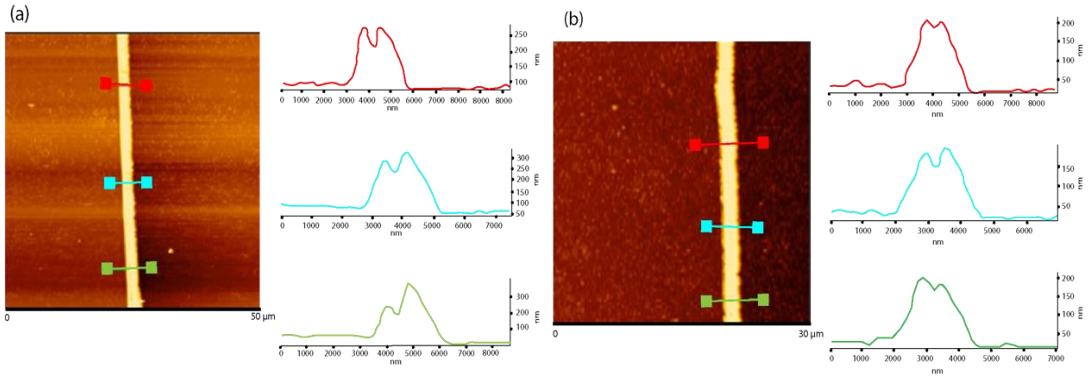

Figure 48. AFM measurements of S22 sample (a) before etching and (b) after 9 min etching.

When the AFM measurements were examined, it was observed that the overlapped fiber thicknesses were approximately 250 nm before the etching process. After the etching process, the overlapped fiber thicknesses were approximately 165 nm. The width of the overlapped fibers is 2.5 µm on average, and there is no change after the etching stage. In the etching process, all the metal in the non-fiber-coated area was removed. A micrometer-sized interdigitated electrode was obtained with metal protected by the polymer pattern.

3.6. Removal of Polymer Studies

In this step, it was tried to determine the duration to remove the polymer on the obtained patterns. The removal of polymer process was performed with a methanol-water solution.

The removal of polymer process was performed on the $Si/SiO_2/Ag$ sample (patterned at 0.4 kV, 700 mm/min platform speed, 1 µl/h syringe pump feed rate) for 5 min. However, it was noticed that a sufficient amount of polymer was not removed from the surface by AFM measurements. The removal of polymer procedure was repeated and the removal of polymer process was carried out for a total of 14 minutes (5+5+2+2 minutes). According to the AFM measurements, the thickness and width of the metallic electrodes from 107 data points were calculated as 102.04 ± 14.40 nm and 473.83 ± 130.39 nm, respectively (Noori et al., 2021).

The removal of polymer process was gradually performed on the Cr/Au sample (patterned at 0.8 kV, 160 mm/min platform speed, 1 µL/h syringe pump feed rate) for a total of 40 min. The thickness and width of the sample, which was 165 nm and 2.5 µm after etching, decreased to 110 nm and 1.85 µm after 40 minutes of removal of polymer process, respectively (See Figure 49). The decrease in width and thickness of the patterns indicated that the polymer was removed by the removal process.

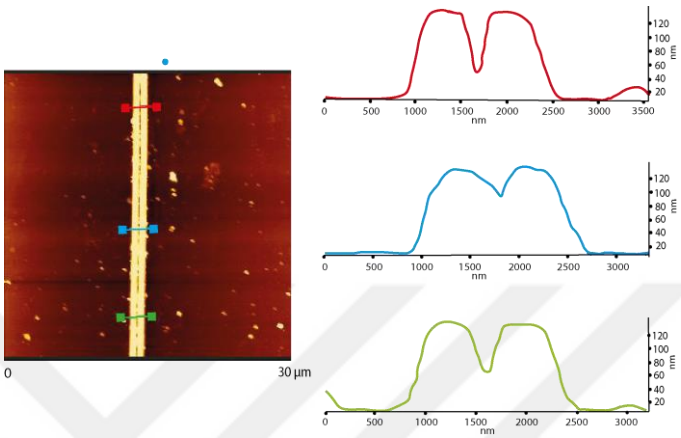

Figure 49. AFM measurements of S22 sample after 40 minutes removal of polymer process.

3.7. Electrical Characterization

IV measurement was performed for electrical characterization. The resistance value of the produced electrodes was calculated using the obtained I-V curve graph.

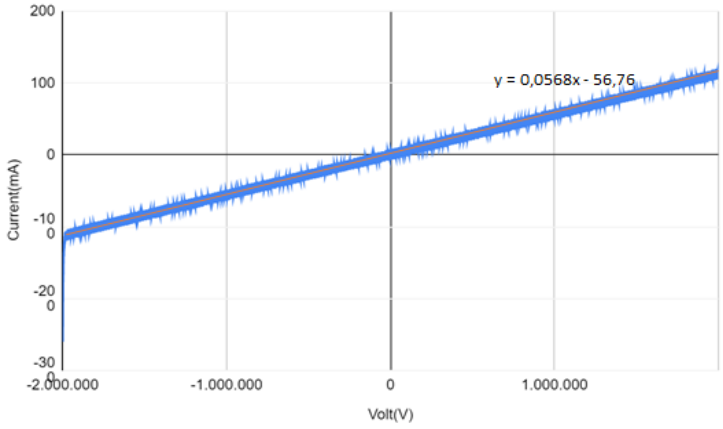

Figure 50. IV curve of S22 sample obtained by two-point probe method.

As shown in the graph, a voltage was applied in the range of [-2, 2] V. The slope of the line in the I-V graph is equal to 1/R. There is an inverse ratio between resistance and slope. Therefore, the I-V plot of a high-value resistor has a low slope,

and the I-V plot of a low-value resistor has a high slope. Since the slope value of the I-V curve graph was 0.0568, the mean resistance value was calculated as 0.0176 Ω. It has been observed that the electrode with micro ranges in the interdigitated arrangement produced with this system has low resistance. The resistance value was low due to the dimensions of the gold interdigitated pattern extending in long strips with a low cross-sectional area. The very low resistance value shows that have obtained a very good conductor.

CHAPTER 4: CONCLUSION

In this study, a platform moving in the x-y axis was combined with the traditional electrohydrodynamic method. The fibers produced in this way are aligned on various substrates, creating different patterns. Then, the regions without fiber were etched with the help of Argon ion etching. After removing the fibers from the surface, an alternative, inexpensive and fast submicron electrode production and alignment method have been developed. The studies can be summarized in two main parts. In the first part, flat fibers were produced by optimization of parameters. In this regard, 100 nm silver-coated silicon dioxide substrates were used in the first stage. In order to draw flat and nano-level fibers on this substrate with the electrohydrodynamic technique, besides many factors, the main focus was on factors such as the distance between the needle tip and the collector, the voltage difference, and the speed of the platform. As a result of these studies, it was understood that the desired structure and thickness fiber production was obtained by analysis of SEM images in the case where the distance is 1 mm, the voltage difference is in the range of 0.4-0.6 kV and the platform speed is 700 mm/min. In the EDX analysis, it was understood that the silver was not determined in the part without fiber after 7 minutes of etching. AFM analyzes were performed before and after etching to more precisely determine the thickness of the fibers. Fiber thickness and diameter before argon ion etching were 93.47 ± 26.96 nm and 715.63 ± 299.6 nm, respectively (calculated from 72 data points). On the other hand, after 7 minutes of argon ion etching, the nanofibers had a thickness of 117.36 ± 33.43 nm and a diameter of 518.98 ± 193.79 nm (calculated from 108 data points) and the etching process also removes a part of the fiber.

In the second part, electrode production in interdigitated order was performed with glass substrates produced by coating 10 nm Cr and 100 nm Au using a magnetic sputtering method. As a result of the studies performed with Ag coated SiO2 substrates, the desired results were achieved when the voltage difference was below 1 kV and the distance between the needle tip and the collector was kept 1 mm. The desired patterning results have reached on a glass substrate coated with 10 nm Cr +100 nm Au, when the distance between the needle tip and the collector is 1-1.5 mm, the applied voltage is 0.95-1 kV, and the syringe pump speed is 0.95-1µL/h. The platform speed range of 90 -160 mm/min was

determined to be more suitable for patterning in interdigitated structure. First, a line was drawn with the fiber towards the middle of the pattern. Then, the fiber was allowed to continue by returning in the same line. In this way, interdigitated patterning was studied without breaking the jet from the substrate. This situation caused the fibers to be intertwined by fibers failing to follow the same path in the return phase in short-interval patterning. In this regard, the patterns with 2 µm, 5 µm, 10 µm, 100 µm, and 200 µm electrode intervals were used to perform the interdigitated structure, and an interdigitated structure could be formed at 200 µm electrode intervals. After the removal of polymer processes, the polymer on the pattern was removed and the electrodes in the desired pattern were obtained.

In addition, patterning studies were carried out at different temperatures using 2% by weight PEO polymer solution. Fibers dispersed on the surface were obtained due to the substrate temperature changing the viscosity of the polymer solution and evaporating the water in the solution. In addition, bead formations were observed in the fibers. Therefore, the studies were continued at room conditions.

There are various parameters in fiber production by the electrohydrodynamic method. The applied voltage difference is an important parameter and affects the fiber thickness. When the voltage difference is high, the drop accumulated at the needle tip adheres to the substrate surface. If it is too low, the fiber breaks during patterning, and the pattern cannot be formed. In addition, the optimum voltage difference changes depending on the distance between the needle tip and the substrate. There is also a very strong relationship between the guide electrode used and the applied voltage. While the applied voltage should be higher in the needle tip guide electrode method, patterning can be made at lower voltage differences when a conductive sheet is used as the guide electrode. Thinner fiber thicknesses were obtained at lower voltage differences.

The syringe pump speed should be at a flow rate that will not disrupt the fiber structure. At high flow rates, the volume of the droplet accumulating at the needle tip increases rapidly. This changes the distance between the needle tip and the substrate and may cause the drop to stick to the substrate surface.

The viscosity of the polymer used has a huge role in patterning. The studies concluded that the optimum viscosity value for patterning was 28.48 Pa·s, the zero-shear viscosity of 2% PEO solution. Patterning was also possible using a 3% by weight PEO solution. However, the desired thickness and patterns could not be obtained.

In addition to the production of nanofibers in the desired thickness, the most fundamental factor affecting the process and encountered in alignment, which is another important factor, is the problem of air conditioning of the room conditions. For example, in the summer months when the room temperature is high, it is not possible to work in the previously obtained optimum conditions (flow rate and voltage difference) due to the decrease in the viscosity of the polymer. This led to problems with alignment. In cold weather, difficulties in forming the fiber due to the freezing of the polymer and increasing its viscosity, and the inability of the fiber to adhere to the substrate surface have occurred. Air conditioning devices (e.g. air conditioners, fans, etc.) also cause airflows in the environment, causing the fiber to break or create irregularities during patterning. For this reason, it is thought that in the future, when the system is moved to an environment where temperature and humidity can be controlled, such as cleanroom conditions, and also placed in a cabinet, the uncontrolled patterning can be overcome and the system can work more efficiently. In addition to this, another factor is that the stage of forming the polymer jet with the probe depends on the human factor. This situation raises concerns about changing the thickness of the polymer jet and forming more than one fiber. In this context, integrating another system that will automatically draw fiber from the drop accumulated on the needle tip with the probe will eliminate this problem and minimize the errors in patterning.

As a result, this method can be presented as an alternative method when electrode positioning is not required at the nanometric level. Although the system components are cheap and fast, and that it does not require gradual processing like optical lithography are the plus points of the method, the sensitivity obtained in electron beam lithography could not be achieved in patterning. The reason for this is that the distance between the electrodes is up to 200 µm due to the fiber structure. However, when the electrical characterization of the electrodes in the interdigitated arrangement obtained in these dimensions was made, the mean resistance value was calculated to be 0.0176 Ω. It has been observed that the electrodes with micrometer intervals in the interdigitated structure produced have low resistance. The resistance

value was low due to the dimensions of the gold interdigitated pattern extending in long strips with a low cross-sectional area. The found very low resistance value shows that we have obtained a very good conductor for nanomanufacturing.

REFERENCES

Agarwal, S., Greiner, A. and Wendorff, J. H. (2009). *Electrospinning of manmade and biopolymer nanofibers—progress in techniques, materials, and applications.* Advanced functional materials, Vol. 19(18), pp. 2863-2879.

Agarwal, S., Wendorff, J. H. and Greiner, A. (2008*). Use of electrospinning technique for biomedical applications*. Polymer, Vol. 49(26), pp. 5603-5621.

Alaboz, H., Demirhan, Y., Yuce, H., Aygun, G. and Ozyuzer, L. (2017). *Comparative study of annealing and gold dopant effect on DC sputtered vanadium oxide films for bolometer applications*. Optical and Quantum Electronics, Vol. 49(7), pp. 1-10.

Atay, E. and Altan A. (2019). *Proses parametreleri ve çözelti özelliklerinin koaksiyal elektropüskürtme yöntemi ile elde edilen nanopartiküllerin morfolojik özellikleri üzerine etkisi*, Gıda 44 (3), pp. 534-551.

Barnes, C. P., Scott, A. S., Sell, S. A., Boland, E. D., Simpson, D. G. and Bowlin, G. L. (2007). *Nanofiber technology: designing the next generation of tissue engineering scaffolds*. Advanced Drug Delivery Reviews, Vol. 59(14), pp. 1413–1433.

Basaran, O. A. (2002). *Small-scale free surface flows with breakup: Drop formation and emerging applications*. American Institute of Chemical Engineers. AIChE Journal, Vol. 48(9), p. 1842.

Bellardita, M., Di Paola, A., Yurdakal, S. and Palmisano, L. (2019). *Preparation of catalysts and photocatalysts used for similar processes*. Heterogeneous Photocatalysis, Elsevier, pp. 25-56.

Bhardwaj, N. and Kundu, S. C. (2010). *Electrospinning: a fascinating fiber fabrication technique.* Biotechnology Advances, Vol. 28, pp. 325–347.

Bhushani, J. A. and Anandharamakrishnan, C. (2014). *Electrospinning and electrospraying techniques: Potential food based applications.* Trends in Food Science & Technology, Vol. 38(1), pp. 21-33.

Bisht, G. S., Canton, G., Mirsepassi, A., Kulinsky, L., Oh, S., Dunn-Rankin, D. and Madou, M. J. (2011). *Controlled continuous patterning of polymeric nanofibers on three-dimensional substrates using low-voltage near-field electrospinning*. Nano letters, Vol. 11(4), pp. 1831-1837.

Bowen, W. R. and Hilal, N. (2009). *Atomic force microscopy in process engineering: An introduction to AFM for improved processes and products*. Butterworth-Heinemann.

Buer, A., Ugbolue, S. C. and Warner, S. B. (2001). *Electrospinning and properties of some nanofibers.* Textile Research Journal, Vol. 71(4), pp. 323–328.

Burger, C., Hsiao, B. S. and Chu, B. (2006). *Nanofibrous materials and their applications*. Annu. Rev. Mater. Res., Vol. 36, pp. 333-368.

Casper, C. L., Stephens, J. S., Tassi, N. G., Chase, D. B. and Rabolt, J. F. (2004). *Controlling surface morphology of electrospun polystyrene fibers: effect of humidity and molecular weight in the electrospinning process*. Macromolecules, Vol. 37(2), pp. 573–578.

Castilho, M., Feyen, D., Flandes-Iparraguirre, M., Hochleitner, G., Groll, J., Doevendans, P. A., and Malda, J. (2017). *Melt electrospinning writing of poly-Hydroxymethylglycolide-co-ε-Caprolactone-based scaffolds for cardiac tissue engineering*. Advanced healthcare materials, Vol. 6(18), p. 1700311.

Chang, C., Limkrailassiri, K. and Lin, L. (2008). *Continuous near-field electrospinning for large area deposition of orderly nanofiber patterns*. Applied Physics Letters, Vol. 93(12), p. 123111.

Chang, J. P., Lin, Y. S. and Chu, K. (2001). *Rapid thermal chemical vapor deposition of zirconium oxide for metal-oxide-semiconductor field effect transistor application.* Journal of Vacuum Science & Technology B: Microelectronics and Nanometer Structures Processing, Measurement, and Phenomena, Vol. 19(5), pp. 1782-1787.

Chekurov, N., Grigoras, K., Peltonen, A., Franssila, S. and Tittonen, I. (2009). *The fabrication of silicon nanostructures by local gallium implantation and cryogenic deep reactive ion etching*. Nanotechnology, Vol. 20(6), p. 065307.

Chen, X., Guo, S., Li, J., Zhang, G., Lu, M. and Shi, Y. (2013). *Flexible piezoelectric nanofiber composite membranes as high performance acoustic emission sensors*. Sensors and Actuators A: Physical, Vol. 199, pp. 372-378.

Chen, Z., Yang, T., Shi, H., Wang, T., Zhang, M. and Cao, G. (2017). *Single Nozzle Electrospinning Synthesized MoO2@ C Core-Shell Nanofibers with High Capacity and Long-Term Stability for Lithium-Ion Storage.* Advanced Materials Interfaces, Vol. 4(3), No. 1600816.

Corbin, E. A., Millet, L. J., Pikul, J. H., Johnson, C. L., Georgiadis, J. G., King, W. P. and Bashir, R. (2013). *Micromechanical properties of hydrogels measured with MEMS resonant sensors.* Biomedical microdevices, Vol. 15(2), pp. 311-319.

De Gans, B. J., Duineveld, P. C. and Schubert, U. S. (2004). Inkjet printing of polymers: state of the art and future developments. Advanced materials, 16(3), 203-213.

Dincer, K., Onal, G., Akdemir, A. and Selbes, M. (2016*). Elektro-Eğirme Yöntemiyle Nanofiber Tabakalı Hava Filtresi Üretimi ve Karakterizasyonu.* Selçuk Üniversitesi Mühendislik, Bilim Ve Teknoloji Dergisi, Vol. 4(4), pp. 271-283.

Eaton, P. and West, P. (2010). *Atomic force microscopy*. Oxford university press.

Fedorova, N. and Pourdeyhimi, B. (2007). *High strength nylon micro-and nanofiber based nonwovens via spunbonding.* Journal of applied polymer science, Vol. 104(5), pp. 3434-3442.

Feng, C., Khulbe, K. C. and Matsuura, T. (2010). *Recent progress in the preparation, characterization, and applications of nanofibers and nanofiber membranes via electrospinning/interfacial polymerization.* Journal of Applied Polymer Science, Vol. 115(2), pp. 756-776.

Fong, H., Chun, D. and Reneker, H. (1999). *Beaded nanofibers formed during electrospinning*, Polymer, Vol. 40(16), pp. 4585-4592.

Ford, S. M., Davies, J., Kar, B., Qi, S. D., McWhorter, S., Soper, S. A. and Malek, C. K. (1999). *Micromachining in plastics using X-ray lithography for the fabrication of micro-electrophoresis devices*. Biomech Eng., Vol. 121(1), pp. 13-21

Garcıa, R. and Perez, R. (2002). *Dynamic atomic force microscopy methods*. Surface science reports, Vol.47(6-8), pp. 197-301.

Garg, T., Rath, G. and Goyal, A. K. (2015). *Biomaterials-based nanofiber scaffold: targeted and controlled carrier for cell and drug delivery*. Journal of drug targeting, Vol. 23(3), pp. 202-221.

Geng, X. Y., Kwon, O. H. and Jang, J. H. (2006). *Electrospinning of chitosan dissolved in concentrated acetic acid solution.* Biomaterials, Vol. 26(27), pp. 5427- 5432.

Ginger, D. S., Zhang, H. and Mirkin, C. A. (2004). *The evolution of dip-pen nanolithography.* Angewandte Chemie International Edition, Vol. 43(1), pp. 30-45.

Goddard III, W. A., Brenner, D., Lyshevski, S. E. and Iafrate, G. J. (2012). *Handbook of nanoscience, engineering, and technology.* 1st Edition. Boca Raton: CRC press.

Graham K., Ouyang M., Raether T., Grafe T., McDonald B. and Knauf P. (2002). *Polymeric nanofibers in air filtration applications*". Fifteenth Annual Technical Conference & Expo of the American Filtration & Separations Society.

Greiner, A. and Wendorff, J. H. (2007). *Electrospinning: a fascinating method for the preparation of ultrathin fibers.* Angewandte Chemie International Edition, Vol. 46(30), pp. 5670-5703.

Guo, L. J. (2007). *Nanoimprint lithography: methods and material requirements*. Advanced materials, Vol. 19(4), pp. 495-513.

Gupta, A., Seifalian, A. M., Ahmad, Z., Edirisinghe, M. J. and Winslet, M. C. (2007). *Novel electrohydrodynamic printing of nanocomposite biopolymer scaffolds*. Journal of bioactive and compatible polymers, Vol. 22(3), pp. 265-280.

Hagewood, J. (2004). *Production of polymeric nanofibers*. International Fiber Journal, Vol. 2, pp. 11-14.

Haghi, A. K. and Akbari, M. (2007). *Trends in electrospinning of natural nanofibers*. Physica Status Solidi (A) Applications and Materials, Vol. 204(6), pp. 1830–1834.

Hartman, R. P. A., Brunner, D. J., Camelot, D. M. A., Marijnissen, J. C. M. and Scarlett, B. (1999). *Electrohydrodynamic atomization in the cone–jet mode physical modeling of the liquid cone and jet*. Journal of Aerosol science, Vol. 30(7), pp. 823-849.

Hayati, I., Bailey, A. I. and Tadros, T. F. (1987). *Investigations into the mechanisms of electrohydrodynamic spraying of liquids: I. Effect of electric field and the environment on pendant drops and factors affecting the formation of stable jets and atomization.* Journal of Colloid and Interface Science, Vol. 117(1), pp. 205-221.

He, G., Zheng, G., Zheng, J., Lin, Y., Wei, J., Liu, H. and Sun, D. (2013, April). *Micro/nano structure written via sheath gas assisted EHD jet*. In The 8th Annual IEEE International Conference on Nano/Micro Engineered and Molecular Systems. IEEE. pp. 625-628.

Huang, Z. M., Zhang, Y. Z., Kotaki, M. and Ramakrishna, S. (2003). *A review on polymer nanofibers by electrospinning and their applications in nanocomposites*. Composites science and technology, Vol. 63(15), pp. 2223-2253.

Jang J (2006). *Displays develop a new flexibility*. Materials Today, Vol. 9(4), pp. 46-52

Jayasinghe, S. N. and Edirisinghe, M. J. (2004). *Electric-field driven jetting from dielectric liquids.* Applied physics letters, Vol. 85(18), pp. 4243-4245.

Kameoka, J., Orth, R., Yang, Y., Czaplewski, D., Mathers, R., Coates, G. W. and Craighead, H. G. (2003). *A scanning tip electrospinning source for deposition of oriented nanofibres.* Nanotechnology, Vol. 14(10), p. 1124.

Ki, C. S., Baek, D. H., Gang, K. D., Lee, K. H., Um, I. C. and Park, Y. H. (2005). *Characterization of gelatin nanofiber prepared from gelatin-formic acid solution*. Polymer, Vol. 46(14), pp. 5094-5102.

Kim, G. H., Shin, J. H., An, T. and Lim, G. (2018). *Junction-free flat copper nanofiber network-based transparent heater with high transparency, high conductivity, and high temperature*. Scientific reports, Vol. 8(1), pp. 1-8.

Kim, J. W., Plachetka, U., Moormann, C. and Kurz, H. (2013). *Fabrication of inverse micro/nano pyramid structures using soft UV-NIL and wet chemical methods for residual layer removal and Si-etching*. Microelectronic engineering, Vol. 110, pp. 403-407.

Kim, T. S., Kim, S. M., Jang, Y. H. and Jung, G. Y. (2007). *Increase of light extraction from GaN based light emitting diodes incorporating patterned structure by colloidal lithography*. Applied physics letters, Vol. 91(17), pp. 171114.

Ko, F. K. and Wan, Y. (Eds.) (2014). *Introduction to nanofiber materials*. Cambridge: Cambridge University Press.

Koseoglu, H., Turkoglu, F., Simsek, Y. and Ozyuzer, L. (2011). *The fabrication of THz emitting mesas by reactive ion-beam etching of superconducting Bi2212 with multilayer masks*. Journal of superconductivity and novel magnetism, Vol. 24(1), pp. 1083-1086.

Kwon, K. W., Choi, J. C., Suh, K. Y. and Doh, J. (2011). *Multiscale fabrication of multiple proteins and topographical structures by combining capillary force lithography and microscope projection photolithography.* Langmuir, Vol. 27(7), pp. 3238-3243.

Larrondo, L. S. J. M. and St. John Manley, R. (1981). *Electrostatic fiber spinning from polymer melts. I. Experimental observations on fiber formation and properties*. Journal of Polymer Science: Polymer Physics Edition, Vol. 19(6), pp. 909-920.

Li, D. and Xia, Y. (2004). *Electrospinning of nanofibers: reinventing the wheel.* Advanced materials, Vol. 16(14), pp. 1151-1170.

Li, D., Wang, Y. and Xia, Y. (2003). *Electrospinning of polymeric and ceramic nanofibers as uniaxially aligned arrays.* Nano letters, Vol. 3(8), pp. 1167-1171.

Li, G., Dong, Q., Xin, J., Leung, C. W., Lai, P. T., Wong, W. Y. and Pong, P. W. (2013). *Patterning micro-and nano-structured FePt by direct imprint lithography*. Microelectronic engineering, Vol. 110, pp. 192-197.

Liu, K., Liu, W., Qiu, Y., Kong, B., Sun, Y., Chen, Z. and Cui, Y. (2017). *Electrospun core-shell microfiber separator with thermal-triggered flame-retardant properties for lithium-ion batteries*. Science advances, Vol. 3(1), No. e1601978.

Loh, K. J. H. (2008). *Development of multifunctional carbon nanotube nanocomposite sensors for structural health monitoring*. University of Michigan.

Lu, X., Wang, C., Favier, F. and Pinna, N. (2017). *Electrospun nanomaterials for supercapacitor electrodes: designed architectures and electrochemical performance*. Advanced Energy Materials, Vol. 7(2), No. 1601301.

Megelski, S., Stephens, J. S., Chase, D. B. and Rabolt, J. F. (2002). *Micro-and nanostructured surface morphology on electrospun polymer fibers*. Macromolecules, Vol. 35(22), pp. 8456-8466.

Min, S. Y., Kim, T. S., Kim, B. J., Cho, H., Noh, Y. Y., Yang, H. and Lee, T. W. (2013). *Large-scale organic nanowire lithography and electronics*. Nature communications, Vol. 4(1), pp. 1-9.

Minden-Birkenmaier, B. A., Selders, G. S., Fetz, A. E., Gehrmann, C. J. and Bowlin, G. L. (2017). *Electrospun systems for drug delivery*. In Electrospun Materials for Tissue Engineering and Biomedical Applications. Woodhead Publishing. pp. 117-145

Mit-Uppatham C., Nithitanakul, M. and Supaphol, P. (2005) *Ultrafine electrospun polyamide-6 fibers: effect of solution conditions on morphology and average fiber diameter*, Macromolecular Chemical Physics, Vol. 205(17), pp. 2327-2338.

Niu, H., Wang, X., Lin, T. (2011). *Needleless electrospinning: Developments and performances, in Lin T. (ed.)* Nanofibers: Production, properties and functional applications, InTech, pp. 17-35.

Noori, A., Döğer, H., Demirhan, Y., Ozdemir, M., Ozyuzer, L., Aygun, G. and Sağlam, Ö. (2021). *Nanolitography based on electrospun and etched nanofibers*. Microelectronic Engineering, Vol. 239, No. 111526.

Park, J. U., Hardy, M., Kang, S. J., Barton, K., Adair, K., kishore Mukhopadhyay, D. and Rogers, J. A. (2007). *High-resolution electrohydrodynamic jet printing*. Nature materials, Vol. 6(10), pp. 782-789.

Park, J. U., Lee, J. H., Paik, U., Lu, Y. and Rogers, J. A. (2008). *Nanoscale patterns of oligonucleotides formed by electrohydrodynamic jet printing with applications in biosensing and nanomaterials assembly*. Nano letters, Vol. 8(12), pp. 4210-4216.

Pfeiffer, H. C. (2010). *Direct write electron beam lithography: a historical overview*. In Photomask Technology 2010. International Society for Optics and Photonics. Vol. 7823, p. 782316

Pimpin, A. and Srituravanich, W. (2012). *Review on micro-and nanolithography techniques and their applications.* Engineering Journal, Vol. 16(1), pp. 37-56.

Pikul, J. H., Graf, P., Mishra, S., Barton, K., Kim, Y. K., Rogers, J. A. and King, W. P. (2011). *High precision electrohydrodynamic printing of polymer onto microcantilever sensors*. IEEE Sensors Journal, Vol. 11(10), pp. 2246-2253.

Popat, K. (Ed.). (2010). *Nanotechnology in Tissue Engineering and Regenerative Medicine.* 1st Edition. Boca Raton: CRC Press.

Qufu, W. (Ed.) (2012). *Functional nanofibers and their applications*. 1st Edition. Philadelphia: Woodhead Publishing.

Ramakrishna, S. (2005). An introduction to electrospinning and nanofibers. Singapore: World Scientific Publishing Co. Pte. Ltd. Available at World scientific books. (Accessed 29 July 2021)

Ramakrishna, S., Fujihara, K., Teo, W. E., Lim, T. C. H. and Ma, Z. (2005). *Basics relevant to electrospinning*. An Introduction to Electrospinning and Nanofibers. Singapore: World Scientific Publishing Co. Pte. Ltd.

Rošic, R., Pelipenko, J., Kocbek, P., Baumgartner, S., Bešter-Rogač, M. and Kristl, J. (2012). *The role of rheology of polymer solutions in predicting nanofiber formation by electrospinning*. European Polymer Journal, Vol. 48, pp. 1374-1384.

Ruiz, S. A. and Chen, C. S. (2007). *Microcontact printing: A tool to pattern*. Soft Matter, Vol. 3(2), pp. 168-177.

Sarbatly R, Krishnaiah D, Kamin Z (May 2016). *A review of polymer nanofibres by electrospinning and their application in oil-water separation for cleaning up marine oil spills*. Marine Pollution Bulletin, Vol. 106(1-2), pp. 8-16.

Schiffman, J. D. and Schauer, C. L. (2008). *A Review: electrospinning of biopolymer nanofibers and their applications.* Polymer Reviews, Vol. 48, pp. 317-352.

Sharifi F, Sooriyarachchi AC, Altural H, Montazami R, Rylander MN, Hashemi N (2016). *Fiber-based approaches as medicine delivery systems*. ACS Biomaterials Science & Engineering, Vol. 2(9), pp. 1411-1431.

Sigmund, W., Yuh, J., Park, H., Maneeratana, V., Pyrgiotakis, G., Daga, A. and Nino, J. C. (2006). *Processing and structure relationships in electrospinning of ceramic fiber systems*. Journal of the American Ceramic Society, Vol. 89(2), pp. 395-407.

Sill, T. J. and Von Recum, H. A. (2008). *Electrospinning: applications in drug delivery and tissue engineering*. Biomaterials, Vol. 29(13), pp. 1989-2006.

Stevenson, J. T. M. and Gundlach, A. M. (1986). *The application of photolithography to the fabrication of microcircuits.* Journal of Physics E: Scientific Instruments, Vol. 19(9), p. 654.

Sun, D., Chang, C., Li, S. and Lin, L. (2006). *Near-field electrospinning*. Nano letters, Vol. 6(4), pp. 839-842.

Sunar, B. S. and Hasçiçek, C. (2017). *Elektroeğrilmiş nanoliflerin ilaç taşıyıcı sistem olarak ve doku mühendisliğinde kullanımı*. Marmara Pharmaceutical Journal, Vol. 21(3), pp. 425-435.

Sylvester, M. A., Amini, F. and Tan, C. K. (2020). *Electrospun nanofibers in wound healing.* Materials Today: Proceedings, Vol. 29, pp. 1-6.

Tan, S. H., Inai, R., Kotaki, M. and Ramakrishna, S. (2005). *Systematic parameter study for ultra-fine fiber fabrication via electrospinning process*. Polymer, Vol. 46(16), pp. 6128-6134.

Tavsanoglu, T. (2009). *Deposition and characterization of single and multilayered boron carbide and boron carbonitride thin films by different sputtering configurations*. Doctoral Thesis. École Nationale Supérieure des Mines de Paris.

Taylor, G. I. (1964). *Disintegration of water drops in an electric field*. Proceedings of the Royal Society of London. Series A. Mathematical and Physical Sciences, Vol. 280(1382), pp. 383-397.

Taylor, G. I. (1969). *Electrically driven jets*. Proceedings of the Royal Society of London. A. Mathematical and Physical Sciences, Vol. 313(1515), pp. 453-475.

Theron, A., Zussman, E. and Yarin, A. L. (2001). *Electrostatic field-assisted alignment of electrospun nanofibres*. Nanotechnology, Vol. 12(3), p. 384.

Thompson, C. J., Chase, G. G., Yarin, A. L. and Reneker, D. H. (2007). *Effects of parameters on nanofiber diameter determined from electrospinning model*. Polymer, Vol. 48(23), pp. 6913-6922.

Thornton, J. A. (1983*). Plasma-assisted deposition processes: theory, mechanisms and applications*. Thin Solid Films, Vol. 107(1), pp. 3-19.

Torres-Martínez, E., Pérez-González, G. L., Serrano-Medina, A., Grande, D., Vera-Graziano, R., Cornejo-Bravo, M. and Villarreal-Gómez, L. J. (2019). *Drugs loaded into electrospun polymeric nanofibers for delivery.* Journal of Pharmacy and Pharmaceutical Sciences, Vol. 22, pp. 313-331.

Tseng, A. A., Chen, K., Chen, C. D. and Ma, K. J. (2003). *Electron beam lithography in nanoscale fabrication: recent development.* IEEE Transactions on electronics packaging manufacturing, Vol. 26(2), pp. 141-149.

Turkoglu, F., Koseoglu, H., Zeybek, S., Ozdemir, M., Aygun, G. and Ozyuzer, L. (2018). *Effect of substrate rotation speed and off-center deposition on the structural, optical, and electrical properties of AZO thin films fabricated by DC magnetron sputtering*. Journal of Applied Physics, Vol. 123(16), pp. 165104.

Unlu, C. G., Li, Z. A., Acet, M. and Farle, M. (2016). *Gas-phase synthesis of Fe-Bi metastable and dumbbell particles*. Crystal Research and Technology, Vol. 51(5), pp. 333-336.

Vasita R, Katti DS (2006). *Nanofibers and their applications in tissue engineering*. International Journal of Nanomedicine, Vol. 1 (1), pp. 15–30

Venugopal, G., Jung, M. H., Suemitsu, M. and Kim, S. J. (2011). *Fabrication of nanoscale three-dimensional graphite stacked-junctions by focused-ion-beam and observation of anomalous transport characteristics*. Carbon, Vol. 49(8), pp. 2766-2772.

Wang, X., Drew, C., Lee, S. H., Senecal, K. J., Kumar, J. and Samuelson, L. A. (2002). *Electrospun nanofibrous membranes for highly sensitive optical sensors*. Nano Letters, Vol. 2(11), pp. 1273-1275.

Wang, Y. F., Chang, X., Zhang, X., Fu, J., Fan, S., Bu, R. and Wang, J. (2018). *Normally-off hydrogen-terminated diamond field-effect transistor with Al_2O_3 dielectric layer formed by thermal oxidation of Al*. Diamond and Related Materials, Vol. 81, pp. 113-117.

Wang, Y., Shahid, M., Cheng, J., Nishijima, H. and Pan, W. (2017). *Electrospun assembly: a nondestructive nanofabrication for transparent photosensors*. Nanotechnology, Vol. 28(15), p. 155202.

Wu, Q., Miao, W. S., Gao, H. J. and Hui, D. (2020). *Mechanical properties of nanomaterials: A review*. Nanotechnology Reviews, Vol. 9(1), pp. 259-273.

Yin Z.P., Huang Y.A., Bu N.B., Wang X.M. and Xiong Y.L. (2010). *Inkjet printing for flexible electronics: materials, processes and equipments*. Chin Sci Bull, Vol. 55(30), pp. 3383-3407

Yuan, X., Zhang, Y., Dong, C. and Sheng, J. (2004). *Morphology of ultrafine polysulfone fibers prepared by electrospinning*. Polymer International, Vol. 53, pp. 1704-1710.

Yuce, H., Alaboz, H., Demirhan, Y., Ozdemir, M., Ozyuzer, L. and Aygun, G. (2017). *Investigation of electron beam lithography effects on metal–insulator transition behavior of vanadium dioxide*. Physica Scripta, Vol. 92(11), pp. 114007.

Yuce, H., Aygun, G., Ozyuzer, L. and Koklu, M. (2015, May*). Characterization of VO 2 films grown by magnetron sputtering*. In 2015 IEEE International Conference on Plasma Sciences (ICOPS). IEEE, pp. 1-1

Zhang, B., Kang F., Tarascon J.M. and Kim J.K. (2016). *Recent advances in electrospun carbon nanofibers and their application in electrochemical energy storage*. Progress in Materials Science, Vol. 76, pp. 319-380.

Zhang, Y., Lim, C. T., Ramakrishna, S. and Huang, Z. M. (2005). *Recent development of polymer nanofibers for biomedical and biotechnological applications.* Journal of materials science: materials in medicine, Vol. 16(10), pp. 933-946.

Zheng, Y. and Zeng, Y. (2014). *Electric field analysis of spinneret design for multihole electrospinning system*. Journal of Materials Science, Vol. 49(5), pp. 1964-1972.

Zhong, Q., Inniss, D., Kjoller, K. and Elings, V. (1993). *Fractured polymer/silica fiber surface studied by tapping mode atomic force microscopy*. Surface Science Letters, Vol. 290(1), p. L688.